VOLUME 33 JULY 1955 NUMBER 7

Canadian Journal of Physics

Published by THE NATIONAL RESEARCH COUNCIL
OTTAWA CANADA

CANADIAN JOURNAL OF PHYSICS

(Formerly Section A, Canadian Journal of Research)

Under the authority of the Chairman of the Committee of the Privy Council on Scientific and Industrial Research, the National Research Council issues THE CANADIAN JOURNAL OF PHYSICS and six other journals devoted to the publication, in English or French, of the results of original scientific research. Matters of general policy concerning these journals are the responsibility of a joint Editorial Board consisting of: members representing the National Research Council of Canada; the Editors of the Journals; and members representing the Royal Society of Canada and four other scientific societies.

Manuscripts for publication should be submitted to Dr. Léo Marion, Editor-in-Chief, Canadian Journal of Physics, National Research Council, Ottawa 2, Canada.
(For instructions on preparation of copy, see **Notes to Contributors** (inside back cover).)

Proof, correspondence concerning proof, and orders for reprints should be sent to the Manager, Editorial Office (Research Journals), Division of Administration, National Research Council, Ottawa 2, Canada.

Subscriptions, renewals, requests for single or back numbers, and all remittances should be sent to Division of Administration, National Research Council, Ottawa 2, Canada. Remittances should be made payable to the Receiver General of Canada, credit National Research Council.

The journals published, frequency of publication, and prices are:

Canadian Journal of Biochemistry and Physiology	Bimonthly	$3.00 a year
Canadian Journal of Botany	Bimonthly	$4.00 a year
Canadian Journal of Chemistry	Monthly	$5.00 a year
Canadian Journal of Microbiology*	Bimonthly	$3.00 a year
Canadian Journal of Physics	Monthly	$4.00 a year
Canadian Journal of Technology	Bimonthly	$3.00 a year
Canadian Journal of Zoology	Bimonthly	$3.00 a year

The price of single numbers of all journals is 75 cents.

*Volume 1 will combine three numbers published in 1954 with six published in 1955 and will be available at the regular annual subscription rate of $3.00.

Canadian Journal of Physics

Issued by THE NATIONAL RESEARCH COUNCIL OF CANADA

VOLUME 33 JULY 1955 NUMBER 7

A CALORIMETRIC DETERMINATION OF THE AVERAGE KINETIC ENERGY OF THE FRAGMENTS FROM U^{235} FISSION[1]

BY R. B. LEACHMAN AND W. D. SCHAFER

ABSTRACT

The average heat of thermal-neutron induced fission of U^{235} has been measured by a differential calorimeter. The average energy per fission observed by the calorimeter was 170.1 ± 1.2 Mev. On the basis of the thicknesses of the calorimeter materials and the theoretical energy loss equation, the β energy per fission observed by the calorimeter is 3.0 ± 1 Mev. and, on the same basis, the γ and neutron energy observed is negligible. The resulting 167.1 ± 1.6 Mev. for the average kinetic energy of the fission products is shown to be in good agreement with less direct determinations of this quantity.

INTRODUCTION

As Whitehouse (11) has pointed out in his review article on fission, the fission process results in the emission of β particles, γ rays, neutrons, and fission fragments. These fission fragments have a wide range of masses and velocities. In addition, the nuclear charge of fission fragments of a given mass is not fixed and, similarly, the effective charge of the fission fragments in motion is variable.

As a result of these complexities, energy measurements of the fission process have resulted in rather large variations in the measured fission energy. Many ionization chamber measurements have been made of the kinetic energy of the fission products, most recently by Brunton and Hanna (2) and Wahl (9), but these determinations of energy are much lower than that made by Leachman (7) from the velocities of the fission products. The difference between the energy determined by ionization and velocity has been explained on the basis of ionization defects by Knipp and Ling (6).

In addition, the average kinetic energy of the fission fragments has been calculated from the mass equation of fission by Leachman (7). These calculations were recently confirmed by Dube and Singh (3). The calculated energy is in good agreement with the energy determined from velocity measurements.

Although calorimetric determinations of fission energy avoid the difficulties of variations in mass, charge, and velocity encountered in the above measurements and in any energy measurements by deflection techniques, the calorimetric measurements have the uncertainty of the amount of β, γ, and neutron

[1]*Manuscript received February 28, 1955.*
Contribution from the Los Alamos Scientific Laboratory, Los Alamos, New Mexico, U.S.A.
This document is based on work performed under the auspices of the U.S. Atomic Energy Commission.

energy of fission that is observed in the calorimeter. For this reason both the early measurement by Henderson (4) and the recent measurement by Meem (8) are difficult to interpret. The purpose of the present calorimetric measurement is to determine the heat of fission with a small uncertainty in regard to the β, γ, and neutron energy observed.

CALORIMETER

A differential type calorimeter employing a null indication for heat measurement is used in the present measurements. To determine both the heat produced by the fissions and the number of fissions producing the heat, a combination of a calorimeter and a fission pulse counter is used. Although it is desirable to irradiate a large mass of uranium with neutrons to increase the fission heat, the uranium thickness introduces difficulties in neutron absorption in the uranium. To reduce these absorption difficulties and to obtain two simultaneous monitorings of the number of fissions, the calorimeter was designed to provide equal neutron flux incident on monitor foils of uranium on both sides of the uranium metal.

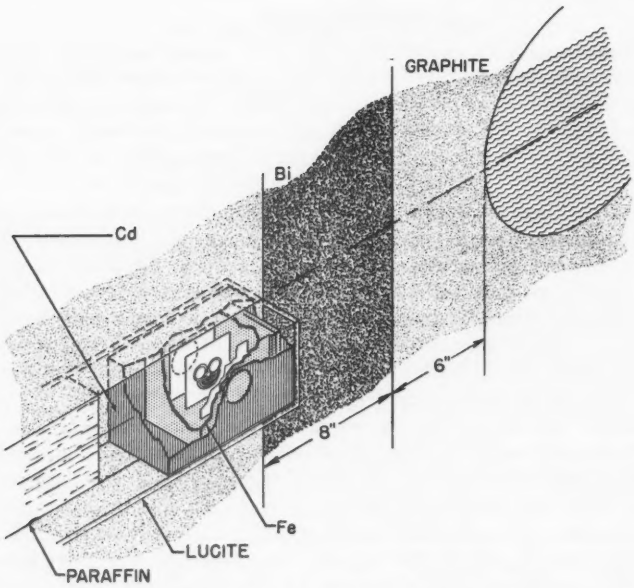

FIG. 1. Schematic diagram of the position of the calorimeter in the thermal column of the reactor with the reactor sphere at the right.

Shown in Fig. 1 is a schematic diagram of the position of the calorimeter in the north thermal column of the Los Alamos Homogeneous Reactor, which has been described by King (5). As shown in the figure, the calorimeter is

separated from the sphere of the reactor, which contains the reacting uranyl nitrate, by 8 in. of bismuth and is surrounded on other sides by graphite and paraffin. Surrounding the calorimeter is a jacket of 1/64-in. cadmium with 2-in. diameter windows on the sides parallel to the monitor foils. By this means, only neutrons that are of nearly normal angle of incidence irradiate the uranium metal in the cells in the center plate of the calorimeter. Measurements made with the calorimeter and earlier measurements made by activation of indium foils indicate that the neutron fluxes through the two windows are equal to within one per cent.

The two outer plates in the calorimeter chamber are the collection plates of the two ionization chambers. Electrical leads to these plates (not shown in the schematic diagram of Fig. 1) go through paraffin to the counting apparatus outside the reactor. Amplifiers of the Los Alamos 101-A design and scalers of the Los Alamos 750 design were used to count the fission pulses.

The center plate of the calorimeter is shown in greater detail in Fig. 2. Two calorimeter cells are mounted on this plate, one containing U^{235} metal and the

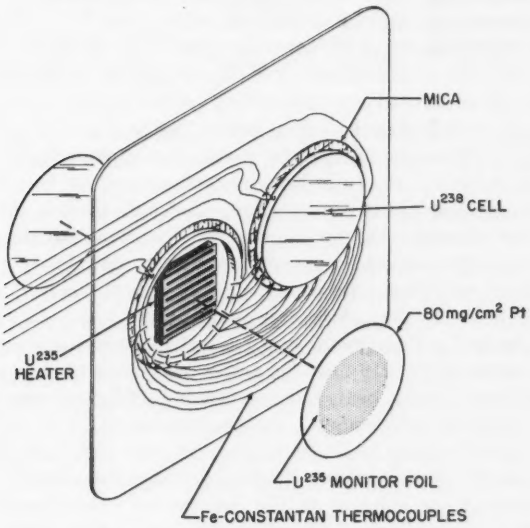

FIG. 2. The center plate of the ionization chamber of the calorimeter with an exploded view of the active calorimeter cell.

other containing U^{238} metal. The cells are 7/8 in. in diameter and are mounted on thin mica rings in 1-in. diameter holes in the plate, which is 2-5/8 in. on each side. The mica was coated with Aquadag and a 0.001-in. platinum wire between the calorimeter cells and the plate assured an equipotential surface. The cells were covered by 80-mgm./cm.^{2} platinum, a thickness that is opaque to fragments from the U^{235} heater. Deposited on the platinum covers of the U^{235} cell were accurately determined monitor masses of 0.7 μgm. of U^{235}.

The chamber was filled to ~15 p.s.i. of argon plus a few per cent of CO_2. A potential of 300 v. was applied across the plates of the chamber for fission counting.

The heaters in the calorimeter cells were fabricated from 0.001-in. uranium metal sliced to provide a continuous strip with a resistance of 36 ohms. The sliced uranium strip was folded back on itself to form a pad four layers thick and 0.5 in. on a side. For the electrical connection to the heaters, short leads of copper wire were copper plated onto the ends of each heater and these connected at the edge of the cell to 0.016-in. nickel wires which led to the seals on the calorimeter case. Nickel wire was chosen as a compromise between heat loss and power loss considerations in these leads. The metal in the U^{235} heater was of 93% isotopic abundance and the mass of the metal was 0.22 gm. Insulating varnish covered the uranium metal, and the heater weight with this insulation was 0.29 gm. The balancing cell of the calorimeter contained U^{238} metal of high isotopic abundance and of similar mass and resistance. At the position of the calorimeter in the thermal column, the neutron spectrum is sufficiently thermalized that the U^{238} fission rate is negligible.

In the measurements, the fission heat generated in the U^{235} cell was matched to equalize the temperature of the two cells. Any temperature difference between the two cells was indicated by a 10-junction iron–constantan differential thermocouple connected to a null reading galvanometer outside the reactor. After the fission rate had been determined by fission counting and the balancing power in the U^{238} cell had been determined, the neutron flux was decreased by a factor of $>10^3$ and electrical heat was substituted for fission heat in the U^{235} cell. This electrical heat required for a null indication is the measure of the fission heat observed by the calorimeter. Precision voltmeters and ammeters were used to measure the power supplied to the cells.

Measurements with the calorimeter indicated that the time constant for increase or decrease of the calorimeter temperature was ~55 sec. The time constant of the null galvanometer was 1.5 sec. Further, the calorimeter sensitivity was found to be 0.18 mw. for 1-mm. deflection of the galvanometer. With the ~46-mw. fission heat, this represented 0.66 Mev. per fission for 1-mm. deflection of the galvanometer. In the design of the calorimeter an effort was made to have the heat loss from each calorimeter cell to the surroundings equal. Unequal heat losses require changes in the power supplied to the U^{238} cell to compensate for changes in the calorimeter case temperature under conditions when power in the U^{235} cell is constant and the cell temperatures are equal. For each degree change in the calorimeter case temperature, the unequal heat losses were found to require a ~0.03-mw. change in the difference between the powers in the two cells for a temperature balance. Since the temperature of the calorimeter case varied by <0.5°C. during the measurements, an error of only 0.03% from this cause is possible.

RESULTS

A typical bias curve of the fission pulses from a monitor foil is shown in Fig. 3. As a result of background conditions in the chamber and irregularities of the surface of the monitor foil, the fission rate of the monitor foils decreases with

increasing bias of the scalers. The masses of the monitor foils were determined in separate measurements by comparing the fission rates of these foils with those of standard foils made by quantitative electrodeposition when both are irradiated simultaneously by the same neutron flux. The position in the reactor and the design of the twin ionization chamber used for the comparison fission counting were both similar to the conditions shown in Fig. 1. In the comparison

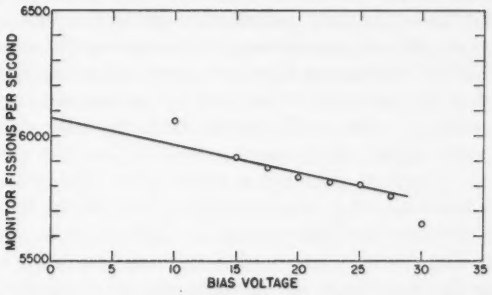

FIG. 3. A typical plateau curve resulting from integral counting of fission pulses greater than the indicated bias. The linear extrapolation to zero bias is indicated. Statistical uncertainties are the size of the datum points.

fission counting, a similar change in fission rate with bias was encountered for the monitor foils, while the bias curve of the standard foils changed by less than one per cent. On this basis the uncertainty in the interpretation of the shape of the bias curves is effectively avoided by referring the extrapolated counting rates of the monitor foils to that of the standard foil.

Throughout the course of the many measurements made with the calorimeter, several determinations of the mass of the monitor foils were made by comparison with standard foils. However, the masses of the monitor foils at the time of the fission heat measurements were used in the determination of the fission energy. Nevertheless, the masses of the monitor foils were reproducible to within three per cent even though the masses could change through the handling necessitated by the mounting and dismounting for these mass measurements. The mass determinations, which were spaced over a period of 10 months, are all listed in chronological order in Table I along with the

TABLE I

DETERMINATIONS OF THE U^{235} MASS ON THE MONITOR FOILS

Standard foil mass (μgm.)	Monitor No. 1 mass (μgm.)	Monitor No. 2 mass (μgm.)
0.13477	0.7256	0.7425
0.13501		0.7211
0.13439	0.7282*	0.7195*
0.13439		0.7190

**Values used for fission heat determinations.*

masses of the standard foils used for comparison. The fission energies calculated from these two monitor masses always agreed within 0.3%, an agreement which indicates that the relative masses of the monitors are correct. In separate measurements the masses of the standard foils have been confirmed by other means, such as α counting and weighing.

In the determination of the energy per fission observed in the calorimeter, several corrections, each of less than one per cent, were necessary. The background rate of the fission chamber, presumably due to uranium contamination in the chamber and γ pile-up, was measured by covering the monitor foils and found to be $\sim$0.5% of the fission rate from the monitor foils. The electrical energy deposited in the nickel leads between the heater and the seal through the calorimeter case and also in the copper leads from the calorimeter case to the meters at the outside of the reactor was 0.5% of the measured power supplied to the U^{235} heater. Because of the neutron absorption in the U^{235} heaters and, to a lesser extent, in the platinum of the monitor foils, the neutron flux observed by the monitor foils was 0.4% higher than the average flux in the U^{235} heater. The neutron attenuation through the cell was determined from the relative fission rates of the monitor foils when windows in the cadmium jacket around the calorimeter were alternately closed. The measured fission rates of the monitor foils were increased by 0.6% to compensate for the fission pulses lost by the 1-μsec. input resolving time of the model 750 scalers. The mass of the monitor foils used in the calorimeter was a compromise between this loss and the desire to have a large monitor mass to reduce possibilities of contamination by handling.

Twenty-seven determinations of the heat of fission were made by this calorimeter, but most of these were taken under questionable conditions. Five determinations were made under apparently ideal conditions. Four of these runs were made with the same gas filling of the chamber, for which only one bias curve was measured. In the evaluation of the data, the remaining run with the separate bias curve was weighted twice as heavily as these four. These data indicated 170.1 Mev. per fission observed in the calorimeter with an uncertainty of $\pm$1.0 Mev. per fission (95% confidence interval). This energy includes the above small corrections. When the estimated uncertainties in these corrections and the uncertainties in the monitor masses are included, the composite uncertainty in the measured energy is $\pm$1.2 Mev. per fission.

DISCUSSION

The amount of the energy of the fission β particles, γ rays, and neutrons observed by the calorimeter is to be taken into account. Way and Wigner (10) show that, on the average, six β particles are emitted in the decay of the fission products of each fission event. For the β energy of fission product decay, Bethe and Ashkin (1) show by theoretical considerations that dE/dx is $\backsim$1 kev./mgm./cm.^{2} in platinum and uranium. On this basis, the average loss of each β particle in the calorimeter, under the assumption of isotropic emission uniformly through the uranium, is estimated to be $\sim$0.29 Mev. Similarly, the average loss in the uranium is $\sim$0.21 Mev. Way and Wigner (10)

calculate that the rate of energy loss by β particles at 5–10 min. after fission (when the fission energy was determined by electrical power substitution) is negligibly small compared to the energy loss during the period of neutron irradiation. Similarly, on the basis of their calculations, the 10–30 min. period of irradiation of the U^{235} in the measurements results in nearly complete build-up of the β activity from fission. As a result, an estimated 0.50 Mev. is lost in the calorimeter by each β particle and 3.0 ± 1 Mev. of β energy for each fission event is observed by the calorimeter. The energy of the fission γ rays and neutrons observed by the calorimeter can be shown to be negligibly small.

With the estimated β energy subtracted, the average kinetic energy of the fission fragments of thermal-neutron induced fission of U^{235} is 167.1 ± 1.6 Mev. This result agrees with 167.1 ± 2 Mev. for fission determination from velocity measurements by Leachman (7). It is significantly larger than the ionization chamber determinations of 154.7 and 149.9 Mev. per fission by Brunton and Hanna (2) and Wahl (9), respectively.

The agreement with the early calorimetric observation of 177 Mev. per fission ($\pm1\%$) by Henderson (4) is satisfactory. Henderson estimated that 12 ± 6 Mev. of β energy was observed by his calorimeter, an estimate which seems high on the basis of the calculations by Way and Wigner (10). More recently, the U^{235} fission energy deposited in a fuel element of the Oak Ridge Bulk Shielding Reactor was determined by Meem (8) to be 193 ± 5 Mev. per fission. This measurement, however, has the uncertainty of the amount of γ-ray energy observed and uncertainties of the cross sections of gold activation and uranium fission involved in the measurements.

On the basis of the uncertainties of the masses and neutron binding energies used in the calculations, the 170 and 171.2 Mev. per fission calculated from the mass equation of fission by Leachman (7) and Dube and Singh (3) respectively, are in satisfactory agreement with the 167.1 ± 1.6 Mev. per fission of the present determination.

ACKNOWLEDGMENTS

The authors wish to acknowledge the co-operation of Mr. G. W. Knobeloch in the comparison fission counting of the monitor foils. The assistance of Mr. B. C. Collins in early work with fission calorimeters is appreciated.

REFERENCES

1. Bethe, H. E. and Ashkin, J. Experimental nuclear physics. Vol. I. John Wiley & Sons, Inc., New York. 1953.
2. Brunton, D. C. and Hanna, G. C. Can. J. Research, A, 28: 190. 1950.
3. Dube, G. P. and Singh, L. S. Indian J. Phys. 28: 227. 1954.
4. Henderson, M. C. Phys. Rev. 58: 774. 1940.
5. King, L. D. P. AECD 3287. Office of Technical Services, Department of Commerce, Washington, D.C. 1951.
6. Knipp, J. K. and Ling, R. C. Phys. Rev. 82: 30. 1951.
7. Leachman, R. B. Phys. Rev. 87: 444. 1952.
8. Meem, J. L. Nucleonics, 12 (No. 5): 62. 1954.
9. Wahl, J. S. Phys. Rev. 95: 126. 1954.
10. Way, K. and Wigner, E. P. Phys. Rev. 73: 1318. 1948.
11. Whitehouse, W. J. Progr. Nuclear Phys. 2: 120. 1952.

A RECORDING MAGNETIC VARIOMETER[1]

By J. H. Meek[2] and F. S. Hector

ABSTRACT

The circuit and detecting head of an electronic recording magnetic variometer are described. The apparatus will give continuous and immediately observable values of variations of magnetic field as small as 10^{-5} oersted, if necessary.

INTRODUCTION

Electronic instruments for measuring small magnetic fields, as required for air-borne magnetic surveys, have been described in the literature, for example Bailey (1) and Wyckoff (4). However there does not appear to have been published a complete description of an electronic magnetometer designed to measure the changes in the earth's magnetic field at one place. Described below is a recording magnetic variometer for use in recording continuously day after day the variations of each of the three components of the earth's magnetic field. In the design of this apparatus the authors are indebted to Dr. P. Serson of the Dominion Observatory, Mr. H. Serson of the Defence Research Board, and Mr. R. Bailey of the National Research Council, for use of unpublished developments in this field.

An instrument is required which will measure variations in magnetic field to a sensitivity of about one gamma. (1 gamma = 10^{-5} oersted.) Normally the instrument will be operated at about one tenth of this sensitivity or 1000 gammas full scale on the recording meter; the extra sensitivity is required to study micropulsations and other minor magnetic variations. The classical suspended magnet magnetometer will achieve the required sensitivity; however it is a delicate instrument and since it records by reflection of a light source on sensitized paper, a darkened room is required to house the apparatus. The record must then be processed before it can be examined.

The saturating core electronic type magnetometer has no moving parts. It can provide more than enough sensitivity. When it is used to measure variations of magnetic field there are very few special requirements for adequate setup. A firm base for the detecting head and a reasonably constant ambient temperature are all that is necessary. Stationary masses of metal or magnets in the vicinity of the head will not affect the recording of variations of a component of the earth's magnetic field. They merely introduce a constant external magnetic field which may be cancelled by a compensating field. We assume, of course, that magnetic potentials at a point are additive and thus also are the components of magnetic field.

The apparatus consists of a detecting head, an amplifying circuit, and a recording meter. A 500 cycle oscillation is applied to two oppositely wound primary coils, each having high permeability cores. An external magnetic

[1]*Manuscript received March 7, 1955.*
Contribution from the Physics Department, University of Saskatchewan, Saskatoon, Saskatchewan.
[2]*Employed by Defence Research Board, Radio Physics Laboratory and seconded to the University of Saskatchewan.*

field is detected in a single secondary winding as a 1000 cycle oscillation. This signal is rectified in a phase sensitive detector and used to control the current in an additional winding which reduces the magnetic field on the cores to zero. The amount of this current is indicated on the recording meter.

THE DETECTING HEAD

The detecting head is illustrated in cross section in Fig. 1.

(*a*) *The Coils*

The primary coil consists of two similar single layer coils (600 turns each #36 wire) wound closely around two "Vycor" glass tubes (1/16 in. O.D., 3 in. long) each containing a length of 0.01 in. permalloy wire. The two

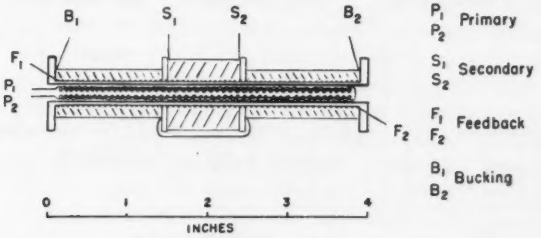

FIG. 1. Diagram of detecting head (approximately to scale).

windings are in opposition so that the fields due to currents flowing in the primary coils are equal and opposite. In order to ensure this, it was necessary to match the two permalloy cores carefully so that they were of equal length and produced complete cancellation.

The feedback coil, a single layer (500 turns #34 wire), is wound on the coil form outside the primary cavity. The sensitivity of the apparatus is varied by adjusting the amount of feedback current.

The secondary coil is wound on the middle 1 in. of the coil form (8000 turns #36 wire). Being short, it should be more sensitive to flux changes in the permalloy core than a full length secondary coil.

The bucking coils (4500 turns each #36 wire) provided to cancel out the average external magnetic field are wound on either side of the secondary and are connected in series.

(*b*) *The Permalloy Cores*

Correspondence with Mr. A. G. Ganz of the Bell Telephone Laboratories and Dr. G. K. Green of the Brookhaven National Laboratories led to the following procedure for making the permalloy cores.

A length of standard 1/4 in. Vycor glass tubing (melting point about 1500°C.) was drawn out to 1/16 in. outside diameter. A piece of 0.01 in. Mo-permalloy wire, obtained from the Bell Telephone Laboratories, was threaded through the tube. Helium gas was passed through the tube while the wire was heated to red through the glass to help drive off the impurities.

The tube was then drawn apart and sealed off at 3-in. intervals. Since the melting point of the permalloy is about 1100°C., the wire separated before the glass melted and sealed off. In order to remove mechanical strains in the cores they were heated to 1000°C. in a furnace and then allowed to cool at 40°C. per hour. This annealing resulted in cores with high permeability and no detectable residual magnetism.

THE CIRCUIT

The electronic circuit is illustrated in Fig. 2. The oscillator circuit, adapted from one described in Reference (2), is a push–pull oscillator operating at about 500 cycles per second. The exact frequency is not critical. It has a low second

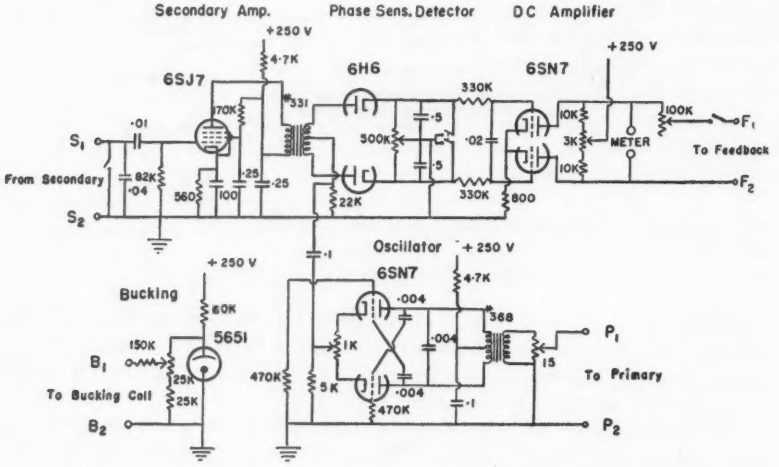

FIG. 2. Recording magnetic variometer.

harmonic output which is very desirable in this application. A 1000 cycle output (double the primary frequency) for the phase sensitive detector is available at the cathodes. The adjustable cathode resistor ensures a good wave shape for the oscillator.

The 500 cycle oscillation is applied to the primary coils of the detecting head. When no external magnetic field is present, no signal is detected by the secondary, as the primary coils are similar and oppositely wound. When an external field does exist, the primary applied magnetic field is shifted with respect to the hysteresis loop of the permalloy cores. As the cores operate in opposite phases, the resultant magnetic flux produces a signal which is detected in the secondary at double the primary frequency. This is amplified and compared with double the oscillator frequency in a phase sensitive detector. The resultant voltage is amplified in a d-c. amplifier. The operating levels of the phase sensitive detector tube and the d-c. amplifier tube are balanced by means of the variable resistors in their respective circuits. The difference

in plate currents of the d-c. amplifier is used (*a*) to provide a feedback current to the feedback winding on the detecting head, (*b*) to operate a 0–1 ma. recording meter. The meter deflection is calibrated to read intensity of magnetic field directly in gammas.

The feedback current is, of course, arranged to oppose the external magnetic field so that the whole circuit operates at a null. The "feedback ratio" is over 20 for normal operating sensitivity, and the feedback current is less than 0.2 ma. The feedback ratio refers to the ratio of the recording meter scale deflection for an applied field of the order of 100 gammas without feedback to that with feedback applied. For good stability this ratio should be as large as possible. A value of 20 is not difficult to achieve and appears to be satisfactory when operating the apparatus at a sensitivity of 1000 gammas full scale. The value of the feedback ratio depends upon (*a*) the make-up of the detecting head, the length of the permalloy cores, and the dimensions and number of turns on each of the coils, (*b*) the amplification of the detector circuit, (*c*) the shapes and amplitudes of the primary oscillations and of the reference oscillations, (*d*) the operating sensitivity of the whole apparatus, which is adjusted by the amount of current fed back to the detecting head. The feedback current is varied by means of a series potentiometer so that the sensitivity of the apparatus is immediately adjustable. The circuit may be used without feedback when long term stability is not required. In this state magnetic fields of the order of one half of a gamma can readily be measured.

The bucking current is obtained by dividing down the voltage from a 5651 voltage regulator tube. The tube is mounted in a thermally insulated can to shut out the light and to eliminate any possible effects on the voltage regulation, of sharp temperature variations. The bucking current at Saskatoon is 0.135 ma. for the horizontal north-pointing component (13,400 gammas at Saskatoon). Owing to the simplicity of its circuit, a constant voltage rather than a constant current is applied to the bucking coil. In a 24-hr. run variations due to the bucking circuit are less than 10 gammas when the apparatus is operated at a sensitivity of 1000 gammas full scale. A temperature variation of 5°F. of the detecting head does not produce as much as 10 gammas variation when operating at the same sensitivity.

A commercial regulated power supply is used operating through a constant voltage transformer, from the 110 volt line. The former regulates the applied high voltage, while the latter maintains a constant voltage on the filaments.

CALIBRATION

The sensitivity of the magnetometer is checked by means of a Helmholtz type coil consisting of two single turn loops, each of 14 cm. radius and placed 16 cm. apart. For calibration the pair of loops is placed over the detecting head and a direct current passed through the two loops in series. It is calculated that a current of 17.1 ma. corresponds to a field of 100 gammas at the center of the Helmholtz pair. The field at the center of one of the loops is 1.5% less than at the center of the pair so that a current of 17.2 ma. per 100 gammas is used for calibrating the magnetometer.

MEASUREMENTS OF THE EARTH'S MAGNETIC FIELD

Continuous records of variations of the earth's magnetic field have been made for some time at Saskatoon. The expansion of the recorder time scale is variable. A record of 2 ft. of paper per day, the same order as that used at permanent magnetic stations, is sufficient at present. A sensitivity of 1000 gammas full scale (about three inches of paper) is satisfactory except on very disturbed days. This is about one third of the sensitivity used at permanent magnetic stations. Owing to the fact that the recording is on a paper strip (requiring no processing before examination) the records have been used successfully at Saskatoon to predict from the magnetic field variations during the afternoon the occurrence of bright auroral displays during the coming night. The main use of the magnetic records has been for correlation with ionospheric and auroral light variations (3).

ACKNOWLEDGMENT

In addition to the persons mentioned in the introduction, we should like to express our appreciation of the interest and advice of Dr. D. M. Hunten of the Physics Department of the University of Saskatchewan.

REFERENCES

1. BAILEY, R. Can. J. Research, A, 26: 523. 1948.
2. CHANCE, B. Waveforms. Mass. Inst. Technol. Radiation Laboratory Series. Vol. 18. McGraw-Hill Book Company, Inc., New York. 1950. p. 423.
3. MEEK, J. H. J. Geophys. Research, 58: 445. 1953.
4. WYCKOFF, R. D. Geophysics, 13: 182. 1948.

THE BETHE–SALPETER EQUATION FOR MANY-BODY SYSTEMS[1]

By R. O. A. Robinson

ABSTRACT

The mathematical technicalities involved in reducing the Bethe–Salpeter equation to the Schrodinger form of a wave equation are simplified by means of a formal modification of the interaction process for systems of many particles. This also makes it possible to carry out the reduction in a unique manner. The consequences of the modification are clearly explained, and it is shown that for atomic systems numerical results remain unchanged to order α^2. There would seem to be some grounds for believing that numerical results remain unchanged to all orders, but no formal proof of this has been achieved.

INTRODUCTION AND SUMMARY

A relativistically covariant equation for the bound states of two particles which interact through a quantized field has been derived by Bethe and Salpeter (8) and its fundamental basis has been investigated by Gell-Mann and Low (5). More recently Hamilton (6) has derived equivalent results by making more ample use of *S*-matrix theory. The equation has become known as the two-body Bethe–Salpeter (or more simply BS) equation. In order to make ready comparison with previous results, a procedure must be found for reducing it to the Schrodinger form of a wave equation, with spin and relativistic corrections contained in the terms of the new hamiltonian. Such a procedure has been given by Salpeter (7) and used to evaluate small corrections to the fine-structure of hydrogen. The static Coulomb interaction is considered to be a suitable first approximation to the full two-body interaction, while an appropriate perturbation method enables the inclusion of retardation and higher-order effects.

The BS equation for three interacting particles, whether fermions or bosons, can be written down by analogy. Wentzel (9) has considered the case of three interacting fermions; but the effect of a Foldy–Wouthuysen (4) transformation on the BS equation is to eliminate spin and relativistic corrections.

A further and stronger objection to the Wentzel reduction is that it is not necessarily unique. The reduced form is valid only if one assumes certain forms for the functions χ_s, and the formalism does not permit the verification or otherwise of the assumptions made. Moreover, the resulting perturbation method is somewhat tedious.

The first objection can be overcome by a careful introduction of the Casimir projection operators as employed by Salpeter. This is done in Section 5 of this paper. The resulting equation has been applied to the study of corrections of electrodynamic origin to the energy levels of the ground states of several small atoms, and the results of this study are being submitted for publication to the *Canadian Journal of Physics* in the form of a Note.

The purpose of this paper is to overcome the second objection by giving a method which is complete in all the above respects, and for which is claimed

[1]*Manuscript received December 7, 1954.*
Contribution from the Department of Mathematics, University of Toronto, Toronto, Ontario.

the additional advantage of simplicity. The procedure involves a formal modification of the simplest two-body interactions only, by introducing what are called instantaneous delta-interactions, i.e. fictitious interactions involving delta functions.

The formalism can be readily extended to treat systems of four or more interacting particles.

The modification is introduced and its consequences fully discussed in Sections 3 and 4, while it is shown in Section 5 that in the case of atomic systems the new method gives results which are equivalent to order α^2 to those given by the conventional method. It has also been found from the calculations on energy levels of small atoms mentioned above that in the cases considered the new method gave results equivalent to order α^3. However, no proof of complete equivalence has been arrived at by the present writer.

1. TWO-BODY BS EQUATION

Before reducing the three-body BS equation it is necessary first to treat the two-body equation by a method which avoids the use of the so-called center-of-mass system. In the two-body problem one replaces the particle coordinates by the total and relative coordinates. In the n-body problem, however, there is a multiplicity of relative coordinates from which to select $n-1$ independent ones; and any selection destroys the symmetry of the transformation.

It is convenient for the present purpose to divide momentum from energy variables: instead of four-vectors $\mathbf{p}$, we use $(\mathbf{p}, E)$ where E denotes energy.

In momentum space the BS equation for two fermions distinguished by subscripts a and b is:

$$[1]\quad \{E_1-H_a(\mathbf{p}_1)\}\{E_2-H_b(\mathbf{p}_2)\}\,\psi(\mathbf{p}_1\mathbf{p}_2;E_1E_2)$$
$$= -(2\pi i)^{-1}\int\int d^3k d\epsilon\,\gamma_4{}^a\gamma_4{}^b\,G(\mathbf{k},\epsilon)\,\psi(\mathbf{p}_1+\mathbf{k},\mathbf{p}_2-\mathbf{k};E_1+\epsilon,E_2-\epsilon),$$

where particle a has momentum-energy $(\mathbf{p}_1, E_1)$ and particle b has momentum-energy $(\mathbf{p}_2, E_2)$. H_a and H_b are Dirac free-particle hamiltonians

$$[2]\qquad \begin{cases} H_a(\mathbf{p}_1) = m_a\gamma_4{}^a+\mathbf{p}_1\,.\,\alpha^a, \\ H_b(\mathbf{p}_2) = m_b\gamma_4{}^b+\mathbf{p}_2\,.\,\alpha^b. \end{cases}$$

For electromagnetic interaction between charges e and $-e$,

$$[3]\qquad \gamma_4{}^a\gamma_4{}^bG(\mathbf{k},\epsilon) = -\frac{e^2}{2\pi^2}\left(\frac{1}{k^2}+\frac{\alpha_i{}^a\alpha_i{}^b}{\epsilon^2-k^2}\right),\quad k^2=|\mathbf{k}|^2.$$

The first member of the right-hand side of this equation describes longitudinal photon exchange, and the second the effect of retardation. Thus, in writing down matrix elements, equation [3] allows a complete mathematical separation of these two types of exchange. Diagrammatically this separation is achieved by using time-ordered Feynman graphs, the first number corresponding to instantaneous exchanges.

Equation [1] must be used to determine the eigenvalues and eigenstates of total energy E where

[4] $$E = E_1+E_2.$$

The constraint [4] is assumed to hold throughout what follows. Moreover, the reduction is carried out in the first instance by neglecting the retardation part of $G(\mathbf{k}, \epsilon)$, which is to be restored subsequently by an appropriate perturbation method.

With this approximation, we define a wave function which depends only on the total energy, viz.:

[5] $$\phi(\mathbf{p}_1\mathbf{p}_2) = \int \psi(\mathbf{p}_1\mathbf{p}_2; E_1E_2)dE_1.$$

As a consequence equation [1] can be rewritten:

[6] $$\{E_1-H_a(\mathbf{p}_1)\}\{E_2-H_b(\mathbf{p}_2)\}\ \psi(\mathbf{p}_1\,\mathbf{p}_2; E_1E_2) = (2\pi i)^{-1}Y_{12}\phi(\mathbf{p}_1\,\mathbf{p}_2)$$

where Y_{12} is an interaction operator, defined by

[7] $$Y_{12}f(\mathbf{p}_1\mathbf{p}_2) = \frac{e^2}{2\pi^2}\int\frac{d^3k}{k^2}f(\mathbf{p}_1+\mathbf{k}, \mathbf{p}_2-\mathbf{k}).$$

Now introducing the Casimir projection operators corresponding to each particle

[8] $$\begin{cases}\Lambda_\pm{}^a(\mathbf{p}_1) = [E_a(\mathbf{p}_1) \pm H_a(\mathbf{p}_1)]/(2E_a(\mathbf{p}_1)),\\ \Lambda_\pm{}^b(\mathbf{p}_2) = [E_b(\mathbf{p}_2) \pm H_b(\mathbf{p}_2)]/(2E_b(\mathbf{p}_2)),\end{cases}$$

where

[9] $$\begin{cases}E_a(\mathbf{p}_1) = (m_a{}^2+p_1{}^2)^{\frac{1}{2}},\\ E_b(\mathbf{p}_2) = (m_b{}^2+p_2{}^2)^{\frac{1}{2}},\end{cases}$$

and writing

$$\Lambda_+{}^a\Lambda_+{}^b\phi = \phi_{++},$$

$$\Lambda_+{}^a\Lambda_-{}^b\phi = \phi_{+-}, \text{ etc.},$$

the following relations can be derived with the help of the Feynman rules for fixing the poles of all propagators that occur:

[10] $$\begin{cases}\{E-E_a(\mathbf{p}_1)-E_b(\mathbf{p}_2)\}\ \phi_{++}(\mathbf{p}_1\mathbf{p}_2) = -\Lambda_+^a(\mathbf{p}_1)\Lambda_+^b(\mathbf{p}_2)\ Y_{12}\phi(\mathbf{p}_1\mathbf{p}_2),\\ \{E+E_a(\mathbf{p}_1)+E_b(\mathbf{p}_2)\}\ \phi_{--}(\mathbf{p}_1\mathbf{p}_2) = \Lambda_-{}^a(\mathbf{p}_1)\Lambda_-{}^b(\mathbf{p}_2)\ Y_{12}\phi(\mathbf{p}_1\mathbf{p}_2),\\ \phi_{+-} = \phi_{-+} = 0.\end{cases}$$

These can be summed with the help of the identity

[11] $$\Lambda_+{}^a\Lambda_+{}^b+\Lambda_+{}^a\Lambda_-{}^b+\Lambda_-{}^a\Lambda_+{}^b+\Lambda_-{}^a\Lambda_-{}^b \equiv 1$$

to yield finally:

$$[12] \quad \{E-H_a(\mathbf{p}_1)-H_b(\mathbf{p}_2)\}\ \phi(\mathbf{p}_1\mathbf{p}_1) = -\{\Lambda_+^a(\mathbf{p}_1)\Lambda_+^b(\mathbf{p}_2)-\Lambda_-^a(\mathbf{p}_1)\Lambda_-^b(\mathbf{p}_2)\}\ Y_{12}\phi(\mathbf{p}_1\mathbf{p}_2).$$

Equation [12] is the required eigenvalue equation for E of the usual wave-mechanical form. However, the frame of reference in which it is to be measured is yet to be specified. In terms of center-of-mass coordinates,

$$\mathbf{p}_1 = \mathbf{p} = -\mathbf{p}_2,$$

it reduces identically to the form derived and discussed by Salpeter.

2. PERTURBATION METHOD

The term $G(\mathbf{k}, \epsilon)$ includes only those graphs describing single or iterated photon exchanges; so that a perturbation method is needed not only to restore that part of equation [3] which has been omitted so far, but also to take into account the other graphs that are relevant to the two-particle scattering process. The procedure to be given now is simpler than others previously suggested, and enables the convenient representation of each additional contribution as a direct change in the hamiltonian.

The following is required. Combining equations [6] and [12]:

$$\psi(\mathbf{p}_1\,\mathbf{p}_2;\, E_1E_2) = -(2\pi i)^{-1}\{E-H_a(\mathbf{p}_1)-H_b(\mathbf{p}_2)\} \times \{E_1-H_a(\mathbf{p}_1)\}^{-1}\{E_2-H_b(\mathbf{p}_2)\}^{-1}\ \chi(\mathbf{p}_1\,\mathbf{p}_2),$$

where

$$\phi(\mathbf{p}_1\mathbf{p}_2) = \{\Lambda_+^a(\mathbf{p}_1)\Lambda_+^b(\mathbf{p}_2)-\Lambda_-^a(\mathbf{p}_1)\Lambda_-^b(\mathbf{p}_2)\}\ \chi(\mathbf{p}_1\mathbf{p}_2).$$

So that selecting $++$ components only (i.e. correct to order α^3, α being the fine-structure constant)

$$[13] \quad \psi(\mathbf{p}_1\,\mathbf{p}_2;\, E_1E_2) = -(2\pi i)^{-1}\{E-E_a(\mathbf{p}_1)-E_b(\mathbf{p}_2)\} \times \{E_1-E_a(\mathbf{p}_1)\}^{-1}\{E_2-E_b(\mathbf{p}_2)\}^{-1}\ \phi(\mathbf{p}_1\,\mathbf{p}_2).$$

Consider now the general situation where G in equation [1] depends on ϵ. The function ψ occurring under the integral sign can be replaced according to [13], and consequently the ϵ-integration can be carried out in full. This leads to an equation of type [6] which can be reduced as before. For G-terms representing small corrections it is unnecessary to retain any but the $++$ components of ϕ and ψ.

The G-term arising from a particular process is most readily written down from consideration of the corresponding Feynman graph. If the graph involves n photon exchanges, then the matrix element can be separated into n^2 parts in the manner of equation [3], and each one of these parts will relate to a particular set of time-ordered graphs which it defines in an obvious way.

For example, consider the irreducible Feynman graph of Fig. 1*A*. If we restrict the photons a and b to be longitudinal (i.e. instantaneously exchanges), then there are two and only two ways in which the process can take place, namely according to the time-ordered diagrams Fig. 1*B* and Fig. 1*C*.†

†*Fig. 1B and Fig. 1C might be called the time-ordered "components" of Fig. 1A. This nomenclature will be used in Section 4.*

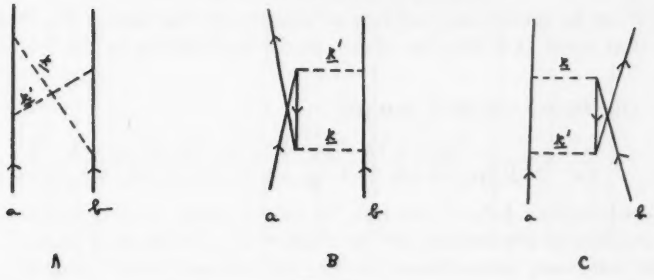

FIG. 1.

The appropriate change in equation [1] is:

$$[14]\quad \{E_1-H_a(\mathbf{p}_1)\}\{E_2-H_b(\mathbf{p}_2)\}\,\psi(\mathbf{p}_1\mathbf{p}_2;E_1E_2)$$
$$=\frac{e^4}{16\pi^6}T'\int\int d\epsilon d\epsilon'\{S_F{}^aS_F{}^b\gamma_4{}^a\gamma_4{}^b\}$$
$$\times\psi(\mathbf{p}_1+\mathbf{k}+\mathbf{k}',\ \mathbf{p}_2-\mathbf{k}-\mathbf{k}';\ E_1+\epsilon+\epsilon',\ E_2-\epsilon-\epsilon'),$$

where T' describes the double longitudinal exchange, viz.:

$$T'=\int\int\frac{d^3k}{k^2}\cdot\frac{d^3k'}{k'^2},$$

and $S_F{}^a$ and $S_F{}^b$ are the propagators

$$S_F{}^a=[(E_1+\epsilon')\,\gamma_4{}^a-(\mathbf{p}_1+\mathbf{k}')_i\gamma_i{}^a-m_a]^{-1},$$
$$S_F{}^b=[(E_2-\epsilon)\,\gamma_4{}^b-(\mathbf{p}_2-\mathbf{k})_i\,\gamma_i{}^b-m_b]^{-1},$$

the summation being taken over $i=1$, 2, and 3. (For purposes of simplicity G-terms considered earlier are omitted from the right-hand side of the last equation [14].)

Equation [14] contains contributions from both Fig. 1*B* and Fig. 1*C*. In order to separate them still further we multiply the expression in curly brackets by the identity [11]. The Dirac matrices are thereby removed from the denominator, since

$$[15]\quad\begin{cases}\Lambda_\pm{}^a(\mathbf{p}_1+\mathbf{k}')\,S_F{}^a\gamma_4{}^a=[E_1+\epsilon'\mp E_a(\mathbf{p}_1+\mathbf{k}')]^{-1}\Lambda_\pm{}^a(\mathbf{p}_1+\mathbf{k}'),\\ \Lambda_\pm{}^b(\mathbf{p}_2-\mathbf{k})\,S_F{}^b\gamma_4{}^b=[E_2-\epsilon\mp E_b(\mathbf{p}_2-\mathbf{k})]^{-1}\Lambda_\pm{}^b(\mathbf{p}_2-\mathbf{k}).\end{cases}$$

Selecting first the contribution $\Lambda_-{}^a\Lambda_+{}^b$, the right-hand side of equation [14] becomes:

$$\frac{e^4}{16\pi^6}T'\int\int\frac{d\epsilon d\epsilon'\,\Lambda_-{}^a(\mathbf{p}_1+\mathbf{k}')\,\Lambda_+{}^b(\mathbf{p}_2-\mathbf{k})\,\psi(E_1+\epsilon+\epsilon',E_2-\epsilon-\epsilon')}{\{E_1+E_a(\mathbf{p}_1+\mathbf{k}')+\epsilon'-i\delta\}\{E_2-E_b(\mathbf{p}_2-\mathbf{k})-\epsilon+i\delta\}},$$

where $\delta>0$, and the momentum arguments of ψ are dropped for purposes of simplicity.

Next ϕ must be substituted for ψ under the integral. The integrations over

ϵ and ϵ' can be carried out, yielding an equation of the form of [6]. Proceeding from that point as before, we obtain finally an addition to the hamiltonian, viz.:

$$[16] \quad \{E-H_a(\mathbf{p}_1)-H_b(\mathbf{p}_2)\}\ \phi(\mathbf{p}_1\mathbf{p}_2)$$
$$= \frac{e^4}{4\pi^4}\ T'\cdot \frac{\Lambda_-{}^a(\mathbf{p}_1+\mathbf{k}')\,\Lambda_+{}^b(\mathbf{p}_2-\mathbf{k})\,\phi(\mathbf{p}_1+\mathbf{k}+\mathbf{k}',\ \mathbf{p}_2-\mathbf{k}-\mathbf{k}')}{E_a(\mathbf{p}_1+\mathbf{k}+\mathbf{k}')+E_a(\mathbf{p}_1+\mathbf{k}')+E_b(\mathbf{p}_2-\mathbf{k})+E_a(\mathbf{p}_1)-E}\ .$$

The contribution $\Lambda_+{}^a\Lambda_-{}^b$ can now be written down from symmetry. These two and similar expressions will be required in a subsequent paper.

The customary association of the plus and minus Casimir projection operators with electrons propagating in positive-energy and negative-energy states respectively would suggest that [16] is the full contribution from the process represented by Fig. 1*B*, and that a similar remark holds good for Fig. 1*C*. However, there is no other possible description of the process; so that with this interpretation, both contributions $\Lambda_+{}^a\Lambda_+{}^b$ and $\Lambda_-{}^a\Lambda_-{}^b$ should vanish identically. It will now be shown that they do.

Returning to equation [14] the $\Lambda_+{}^a\Lambda_+{}^b$ contribution gives on the right-hand side

$$\frac{e^4}{16\pi^6}\ T'\int\int \frac{d\epsilon d\epsilon'\,\Lambda_+{}^a(\mathbf{p}_1+\mathbf{k}')\,\Lambda_+{}^b(\mathbf{p}_2-\mathbf{k})\ \psi(E_1+\epsilon+\epsilon',\ E_2-\epsilon-\epsilon')}{\{E_1-E_a(\mathbf{p}_1+\mathbf{k}')+\epsilon+i\delta\}\{E_2-E_b(\mathbf{p}_2-\mathbf{k})-\epsilon+i\delta\}}\ .$$

Substituting ϕ for ψ, it is found that an expression of the following form must be integrated over ϵ and ϵ':

$$1/(\epsilon'+i\delta+\ldots)(-\epsilon+i\delta+\ldots)(\epsilon+\epsilon'+i\delta+\ldots)(-\epsilon-\epsilon'+i\delta+\ldots).$$

For the $\Lambda_-{}^a\Lambda_-{}^b$ term the analogous form is:

$$1/(\epsilon'-i\delta+\ldots)(-\epsilon-i\delta+\ldots)(\epsilon+\epsilon'+i\delta+\ldots)(-\epsilon-\epsilon'+i\delta+\ldots).$$

Because of the arrangement of the poles of ϵ and ϵ' both integrals vanish.

In practice the interpretation can be put to considerable use. For example, the matrix element for any complex higher-order process can always be broken down into parts in the above manner with the help of equations like [15]; so that quite often many parts can be discarded without calculating them, by simply comparing them with the time-ordered components with which they are associated. In Section 4 this interpretation will frequently be made. In every case it has been verified in detail.

3. MANY-BODY PROBLEM

The obstacle to treating the Wentzel (9) problem is a mathematical one. The basic interactions are two-body interactions, i.e. interactions in which only two of the particles take part, and as a result the matrix elements considered do not contain the same number of propagators for each particle. Details need not be given here. The difficulty is to be overcome by modifying the two-body interactions in a manner that will now be explained.

Consider first the three-body problem; more strictly, the problem of three fermions interacting through the quantized electromagnetic field. If the fermions are distinguished by subscripts *a*, *b*, and *c*, then the basic graphs repre-

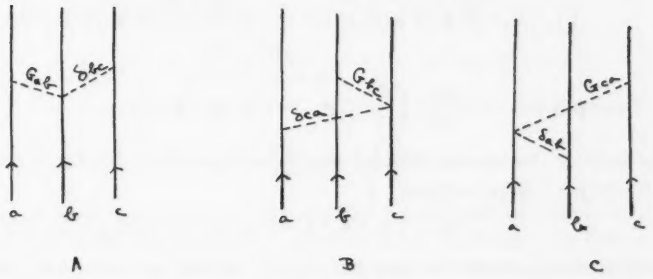

FIG. 2.

sent (i) photon exchange between a and b with c running free, (ii) photon exchange between b and c with a running free, and (iii) photon exchange between c and a with b running free. We refer to the related G-terms respectively as G_{ab}, G_{bc}, and G_{ca}. The lines now to be introduced describe fictitious photon exchanges, the G-term corresponding to a photon of momentum-energy $(\mathbf{k}, \epsilon)$ being $\delta^3\mathbf{k}$. These are to be incorporated according to the following convention: for each G_{ab} exchange add a line δ_{bc}, for each G_{bc} exchange add a line δ_{ca}, and for each G_{ca} exchange add a line δ_{ab}. Finally, the additions must be made in such a way that the δ-line begins at the end of the G-line as shown in Fig. 2. When time-ordering is considered, the exchange of a fictitious photon must be regarded as instantaneous, since the corresponding G-term is independent of the photon energy. (The graphs of Fig. 2 are not time-ordered.)

The three-body BS equation now takes the form:

$$[17] \quad \prod_s \{E_s - H(\mathbf{p}_s)\}\, \psi(E_1E_2E_3)$$

$$= -(2\pi i)^{-1} \int d^3k\, d^3k'\, d\epsilon\, d\epsilon'\, \gamma_4{}^b\gamma_4{}^c\, G_{bc}(\mathbf{k}, \epsilon)\, \delta^3(\mathbf{k}')\, \psi(E_1 - \epsilon', E_2 + \epsilon, E_3 - \epsilon + \epsilon')$$

$$- \cdots - \cdots$$

where, for example,

$$H(\mathbf{p}_1) = m_a\gamma_2{}^a + \mathbf{p}_1.\boldsymbol{\alpha}^a$$

and

$$[18] \qquad \gamma_4{}^b\gamma_4{}^c G_{bc}(\mathbf{k}, \epsilon) = \frac{e_2e_3}{2\pi^2}\left(\frac{1}{k^2} + \frac{\alpha_t{}^b\alpha_t{}^c}{\epsilon^2 - k^2}\right),$$

the electric charges of the respective particles being e_1, e_2, and e_3.

Equation [17] can be treated in a manner exactly similar to that of Section 1. Subject to an obvious extension of equation [4] we define a wave function dependent only on the total energy:

$$\phi(\mathbf{p}_1\mathbf{p}_2\mathbf{p}_3) = \int \psi(E_1E_2E_3)\, dE_1 dE_2 dE_3 \delta(E - E_1 - E_2 - E_3).$$

This leads to:

[19] $$\prod_s \{E_s - H(\mathbf{p}_s)\}\, \psi(E_1E_2E_3) = (2\pi i)^{-1}(Y_{23}+Y_{31}+Y_{12})\phi,$$

where

$$Y_{23} f(\mathbf{p}_1\mathbf{p}_2\mathbf{p}_3) = -\frac{e_2e_3}{2\pi^2}\int \frac{d^3k}{k^2} f(\mathbf{p}_1, \mathbf{p}_2+\mathbf{k}, \mathbf{p}_3-\mathbf{k}), \text{ etc.}$$

With the help of the various Casimir projection operators we obtain finally:

[20] $$\{E - H(\mathbf{p}_1) - H(\mathbf{p}_2) - H(\mathbf{p}_3)\}\, \phi$$
$$= -\{\Lambda_+^a \Lambda_+^b \Lambda_+^c + \Lambda_-^a \Lambda_-^b \Lambda_-^c\}(Y_{23}+Y_{31}+Y_{12})\, \phi,$$

the momentum arguments of Λ and ϕ being omitted for purposes of simplicity.

In the non-relativistic limit equation [20] obviously reduces to the usual Schrodinger equation, provided of course that the center-of-mass frame is specified, viz.:

$$\sum_s \mathbf{p}_s = 0.$$

Furthermore the extension of the above to systems of four or more fermions is immediate. In the four-body problem, for example, we must introduce two fictitious photons for each two-body interaction and in the same cyclic order.

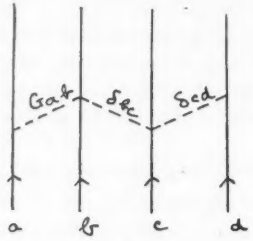

FIG. 3.

As shown in Fig. 3, each δ-line must begin at the end of the previous line. For the remainder of the paper, therefore, only the three-body problem need be discussed.

For the perturbation method we require the analogue of equation [13], and this is obtained from equations [19] and [20], viz.:

[21] $$\psi(E_1E_2E_3) = -(2\pi i)^{-1}\{E - E(\mathbf{p}_1) - E(\mathbf{p}_2) - E(\mathbf{p}_3)\}$$
$$\times \prod_s \{E_s - E(\mathbf{p}_s)\}^{-1} \phi(\mathbf{p}_1\mathbf{p}_2\mathbf{p}_3),$$

where

$$E(\mathbf{p}_1) = (m_a^2 + p_1^2)^{\frac{1}{2}}, \text{ etc.}$$

We proceed to evaluate the correction arising from the second member of [18], which has been omitted so far. Reinstating the appropriate term, equation [17] becomes:

$$\prod_s \{E_s - H(\mathbf{p}_s)\}\ \psi(E_1E_2E_3)$$
$$= -(2\pi i)^{-1} O \int\int \frac{d\epsilon d\epsilon'}{\epsilon^2 - k^2 + i\delta}\ \psi(E_1-\epsilon',\ E_2+\epsilon,\ E_3-\epsilon-\epsilon'),$$

where

[22] $$O = \frac{e_2e_3}{2\pi^2}\alpha_i{}^b\alpha_i{}^c \int d^3k.$$

Other G-terms considered so far are omitted for purposes of simplicity.

Substituting for ψ according to equation [21], the integration over ϵ and ϵ' can be carried out immediately. Then, reducing as before, but retaining only the $++$ components of ϕ and ψ, we obtain finally:

[23] $$\{E - H(\mathbf{p}_1) - H(\mathbf{p}_2) - H(\mathbf{p}_3)\}\ \phi(\mathbf{p}_1, \mathbf{p}_2, \mathbf{p}_3) = OF\phi(\mathbf{p}_1, \mathbf{p}_2+\mathbf{k}, \mathbf{p}_3-\mathbf{k}),$$

where

$$F = \{k^2 - (E(\mathbf{p}_3) - E(\mathbf{p}_3-\mathbf{k}))^2\}^{-1}$$
$$+ \frac{E - E(\mathbf{p}_1) - E(\mathbf{p}_2) - E(\mathbf{p}_3)}{2k\{k + E(\mathbf{p}_3-\mathbf{k}) - E(\mathbf{p}_3)\}\{k + E(\mathbf{p}_1) + E(\mathbf{p}_2) + E(\mathbf{p}_3-\mathbf{k}) - E\}}$$
$$+ \frac{E - E(\mathbf{p}_1) - E(\mathbf{p}_2+\mathbf{k}) - E(\mathbf{p}_3-\mathbf{k})}{2k\{k + E(\mathbf{p}_3) - E(\mathbf{p}_3-\mathbf{k})\}\{k + E(\mathbf{p}_1) + E(\mathbf{p}_2+\mathbf{k}) + E(\mathbf{p}_3) - E\}}.$$

As before the correction is exhibited as an addition to the hamiltonian. Before it is evaluated, the center-of-mass frame of reference must be specified. When this is done the leading term k^{-2} is readily seen to be equivalent to the well-known Breit correction for retardation, while the remainder of F will yield corrections of order α relative to the Breit correction.

Finally, note that the fictitious photon was introduced for the sole purpose of making unique the reduction of the BS equation. For this reason it affects only the basic interactions and iterations of them. When considering corrections due to other types of graph, therefore, it is strictly speaking unnecessary to introduce fictitious photons. Whether they do or do not lead to some simplification will depend on the particular graph under consideration. The discussion of Section 4, where iterations of the basic interactions are considered more fully, will suggest what simplification or otherwise can be expected in the general case.

SECTION 4

The introduction of δ-lines according to the convention given above implies that the new BS equation includes only those ladder-type graphs which are built up from the elementary graphs of Fig. 2.

The point is made clear in Fig. 4. Fig. 4(i) is the usual ladder-type graph describing iteration of the G_{ab}-interaction. Within the new framework, however, there are two possibilities for the same process, and these are shown in Fig. 4(ii) and Fig. 4(iii). In the former the δ-lines do not cross; therefore the graph is reducible, and its contribution is included in equation [17]. In the

latter the δ-lines cross; as a result the graph is not reducible, and it must be treated by the perturbation method as a correction to equation [17]. Finally, the matrix element due to Fig. 4(i) is the sum of the matrix elements due to Fig. 4(ii) and Fig. 4(iii).

If we time-order all the graphs of Fig. 4, it is found that only some of the time-ordered components of (i) are contained in (ii), while the remainder are all contained in (iii), i.e. the essential effect of δ-lines is to reorganize the time-ordering of the usual processes.

Neglecting the retardation part of G_{ab}, i.e. treating the G-lines as instantaneous interactions, Fig. 5 shows the time-ordered components of Fig. 4(ii).

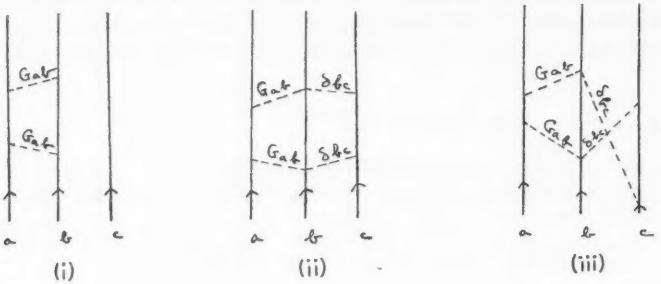

FIG. 4

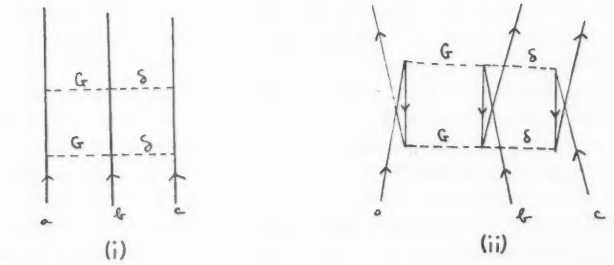

FIG. 5

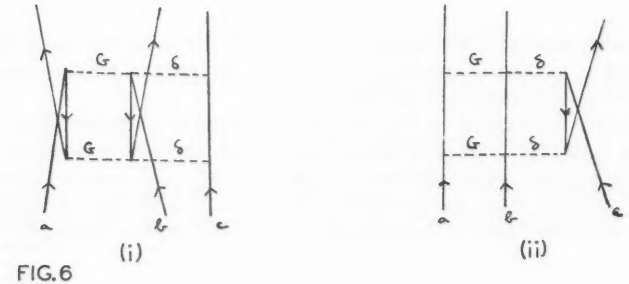

FIG. 6

Similarly Fig. 6 shows the time-ordered components of Fig. 4(iii). (Note that the δ-lines are instantaneous.) Now, since each of these graphs is time-ordered, the removal of the δ-lines will cause no mathematical change in its individual matrix element; so that the time-ordered components of Fig. 4(i) are the graphs of Fig. 5(i) and Fig. 6(i). It is left to show that the contributions from Fig. 5(ii) and Fig. 6(ii) both vanish identically. The result is obvious from the discussion of Section 2. Each of these two graphs contains vertices at which particle c makes a transition from a positive to a negative energy state (or vice versa) and the transition is induced by a δ-interaction. The matrix element for a graph containing any such vertex must vanish, since after integration over energy the vertex gives rise to a product $\Lambda_+{}^c(\mathbf{p})\,\Lambda_-{}^c(\mathbf{p})$ and from equation [8] this product vanishes identically.

To sum up, Fig. 5(i) is included in our wave equation [20], whereas Fig. 6(i) is not. In order to find the correction to the hamiltonian due to the latter graph, it is only necessary to select the contribution $\Lambda_-{}^a\Lambda_-{}^b\Lambda_+{}^c$ from the matrix element for the graph of Fig. 4(iii). Similar results are obtained for the iterated G_{bc} and G_{ca} interactions. The three corrections concerned are of order α^4 or higher.

Corrections of order α^3 arise from analyzing those graphs which describe successive exchanges: e.g. G_{ab} and G_{bc}. We discuss first the ordering $G_{ab}G_{bc}$ (see Fig. 7(i)). The converse ordering can of course be defined and discussed

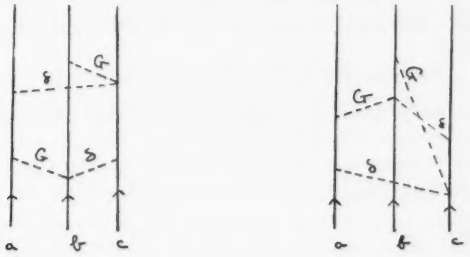

FIG. 7 (i) (ii)

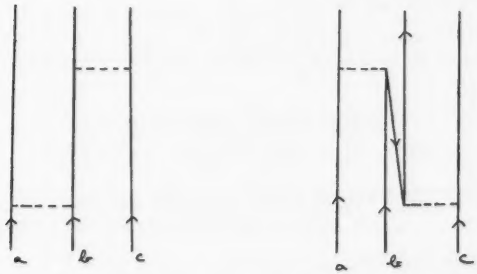

FIG. 8 (i) (ii)

similarly. Introducing the δ-lines there are two topological possibilities as shown in Fig. 7. A simple rule can be given for drawing them: in (i) no two lines intersect; in (ii) δ_{bc} and G_{bc} intersect. No physical significance can be attached to the intersection of other pairs of lines, e.g. of δ_{bc} and δ_{ca}, or of G_{ab} and G_{bc}. In Fig. 7 this is obvious for the second pair, since the fermion line b is placed between the fermion lines a and c. If the graphs are redrawn with the fermion line c placed between the fermion lines a and b, the remark becomes equally obvious for the pair δ_{bc} and δ_{ca}. Other remaining pairs can be disposed of in a similar manner.

Only the first of the graphs of Fig. 7 is reducible and therefore contained in equation [17]. The remainder must be treated as a correction. As before, each of them can be broken down into two time-ordered components. If the G-interactions are regarded as instantaneous, then one component of (i) vanishes, and one component of (ii) vanishes because of products $\Lambda_+\Lambda_-$ arising at certain vertices. The two surviving components are drawn in Fig. 8, where the δ-lines are omitted. Those are clearly the components of the usual graph that describes the iteration under consideration. Fig. 8(i) survives from Fig. 7(i) and is therefore already included in the BS equation. On the other hand, Fig. 8(ii) survives from Fig. 7(ii) and must therefore be treated as a correction. In order to obtain the related correction to the hamiltonian, it is only necessary to select the component $\Lambda_+^a\Lambda_-^b\Lambda_+^c$ from the matrix element for Fig. 7(ii). Analogous corrections arise from studying the ordering $G_{bc}\,G_{ab}$ and other combinations of two G-interactions. The results can be inferred from Fig. 8.

SECTION 5. EQUIVALENCE TO ORDER α^2

In this section the treatment of the three-body system given by Wentzel (9) is extended to include relativistic corrections. Our aim is to show that in the case of atomic systems our equation [20] is equivalent to that now to be derived up to and including terms of order α^2. The steps to be used differ from those of Wentzel's paper only by the use of Casimir projection operators. Equations [25]–[33] below correspond immediately to equations (7)–(17′) of that reference.

The BS equation to be reduced is:

$$[25]\quad \prod_s \{E_s - H(\mathbf{p}_s)\}\,\psi(E_1E_2E_3) = (2\pi i)^{-1}\{E_2 - H(\mathbf{p}_1)\}\,Y_{23}\int d\epsilon\,\psi(E_1, E_2+\epsilon, E_3-\epsilon)+\ldots.$$

Defining

$$[26]\qquad \chi(E_1E_2E_3) = \prod_s \{E_s - H(\mathbf{p}_s)\}\psi$$

we obtain:

$$[27]\quad \chi(E_1E_2E_3) = (2\pi i)^{-1}Y_{23}\int d\epsilon\Bigg\{\frac{\chi_{+++}+\chi_{-++}}{\{E_2+\epsilon-E(\mathbf{p}_2)\}\{E_3-\epsilon-E(\mathbf{p}_3)\}} + \frac{\chi_{++-}+\chi_{-+-}}{\{E_2+\epsilon-E(\mathbf{p}_2)\}\{E_3-\epsilon+E(\mathbf{p}_3)\}} + \frac{\chi_{+-+}+\chi_{--+}}{\{E_2+\epsilon+E(\mathbf{p}_2)\}\{E_3-\epsilon-E(\mathbf{p}_3)\}} + \frac{\chi_{+--}+\chi_{---}}{\{E_2+\epsilon+E(\mathbf{p}_2)\}\{E_3-\epsilon+E(\mathbf{p}_3)\}}\Bigg\}+\ldots$$

where the subscripts + and − indicate the use of the corresponding Casimir projection operators.

It follows from equation [27] that we may write

$$\chi(E_1E_2E_3) = \chi_0 + \sum_s \chi_s(E_s), \tag{28}$$

where

$$\chi_s\{E(\mathbf{p}_s)\} = 0.$$

Omitting from [27] those terms whose numerators involve ϵ, the arrangement of poles causes several terms to vanish, leaving:

$$\chi_0 + \sum_s \chi_s(E_s) = -Y_{23}\frac{P_{+++}+P_{-++}-P_{+--}-P_{---}}{E-E_1-E(\mathbf{p}_2)-E(\mathbf{p}_3)} \tag{29}$$

$$-Y_{31}\frac{Q_{+++}+Q_{+-+}-Q_{-+-}-Q_{---}}{E-E(\mathbf{p}_1)-E_2-E(\mathbf{p}_3)} - Y_{12}\frac{R_{+++}+R_{++-}-R_{--+}-R_{---}}{E-E(\mathbf{p}_1)-E(\mathbf{p}_2)-E_3},$$

where $P = \chi_0+\chi_1(E_1)$, $Q = \chi_0+\chi_2(E_2)$, $R = \chi_0+\chi_3(E_3)$.

Setting $E_s = E(\mathbf{p}_s)$ in equation [29] and making the transformation

$$\{E-H(\mathbf{p}_1)-H(\mathbf{p}_2)-H(\mathbf{p}_3)\}\,\phi = \chi_0 \tag{30}$$

we find:

$$\{E-H(\mathbf{p}_1)-H(\mathbf{p}_2)-H(\mathbf{p}_3)\}\,\phi = -Y_{23}(\phi_{+++}+\phi_{-++}-\phi_{+--}-\phi_{---}) \tag{31}$$
$$-Y_{31}(\phi_{+++}+\phi_{+-+}-\phi_{-+-}-\phi_{---})-Y_{12}(\phi_{+++}+\phi_{++-}-\phi_{--+}-\phi_{---}).$$

The remainder of [29] leads to equations of the type

$$\chi_{1+++}(E_1) = \{E_1-E(\mathbf{p}_1)\}\sum_{n>1}\{-Y_{23}\mathfrak{H}^{-1}(E_1)\}^n\phi_{+++}, \tag{32}$$

where

$$\mathfrak{H}(E_1) = E-E_1-E(\mathbf{p}_2)-E(\mathbf{p}_3), \tag{33}$$

and these can be used to show with little difficulty that those ϵ-dependent terms which were omitted from the right-hand side of equation [27] do in fact vanish.

We go on to show first that equations [20] and [31] are equivalent to order α^2 when applied to atomic systems. For such systems the wave function ϕ is represented correct to order α^3 by the function ϕ_{+++}. Moreover, complex interactions involving two or more Y-interactions lead to corrections of order α^3 or higher. Writing

$$E-E(\mathbf{p}_1)-E(\mathbf{p}_2)-E(\mathbf{p}_3) = H_{+++},$$
$$E+E(\mathbf{p}_1)-E(\mathbf{p}_2)-E(\mathbf{p}_3) = H_{-++}, \text{ etc.},$$

we can break down equation [31] into eight equations as follows:

$$H_{+++}\phi_{+++} = -\Lambda_+^{\,a}\Lambda_+^{\,b}\Lambda_+^{\,c}(Y_{23}+Y_{31}+Y_{12})\,\phi_{+++}$$
$$+ \text{ terms involving } \phi_{++-} \text{ etc.},$$
$$H_{++-}\phi_{++-} = -\Lambda_+^{\,a}\Lambda_+^{\,b}\Lambda_-^{\,c}(Y_{23}+Y_{31}+Y_{12})\,\phi_{+++}$$
$$+ \text{ further terms involving } \phi_{++-} \text{ etc.}$$

We substitute into the first of these equations the values given by the other seven for the remaining components of ϕ. This yields

$$[34] \qquad H_{+++}\phi_{+++} = -\Lambda_+{}^a\Lambda_+{}^b\Lambda_+{}^c(Y_{23}+Y_{31}+Y_{12})\phi_{+++}+O(\alpha^3)$$

where $O(\alpha^3)$ denotes terms involving two or more Y-interactions.

A similar treatment of equation [20] leads to an identical form [34] and hence our result follows.

Furthermore, it is clear from an inspection of the methods of Section 3 as well as of the method outlined by Wentzel for further extension to larger numbers of fermions that the result [34] will continue to hold for both, viz.:

$$H_{++\ldots+}\phi_{++\ldots+\ldots} = -\Lambda_+\Lambda_+\ldots\Lambda_+(Y+Y+\ldots Y)\,\phi_{++\ldots+}+O(\alpha^3).$$

Of course the atomic nucleus is not in general a particle satisfying the Dirac equation; but it is correct to the order required to treat it as a spinless particle. The only modifications required are (i) to replace the associated Casimir projection operators Λ_+ and Λ_- by 1 and 0 respectively, and (ii) to replace Dirac hamiltonians by Schrodinger hamiltonians.

ACKNOWLEDGMENTS

I should like to express my sincere thanks to Mr. J. Hamilton of Christ's College, Cambridge, and to Dr. R. J. Eden of Clare College, Cambridge, for very helpful discussions and criticism.

REFERENCES

1. Breit, G. Phys. Rev. 34: 553. 1929.
2. Chandrasekhar, S., Elbert, D., and Herzberg, G. Phys. Rev. 91: 1172. 1953.
3. Feynman, R. P. Phys. Rev. 76: 749, 769. 1949.
4. Foldy, L. L. and Wouthuysen, S. A. Phys. Rev. 78: 29. 1950.
5. Gell-Mann, M. and Low, F. Phys. Rev. 84: 350. 1951.
6. Hamilton, J. Proc. Cambridge Phil. Soc. 49: 97. 1953.
7. Salpeter, E. E. Phys. Rev. 87: 328. 1952.
8. Salpeter, E. E. and Bethe, H. A. Phys. Rev. 84: 1232. 1951.
9. Wentzel, G. Phys. Rev. 89: 684. 1953.

SCATTERING OF ELECTROMAGNETIC WAVES FROM A "LOSSY" STRIP ON A CONDUCTING PLANE[1]

By James R. Wait[2]

ABSTRACT

One method for solving boundary value problems involving imperfectly conducting media is to assume, for a first approximation, that the surface currents are the same as if the media were perfectly conducting. Using this type of approximation, the problem of a line source of current situated over a plane surface, with a simple type of mixed boundary condition, is solved. For purposes of comparison the situation of an imperfectly conducting or "lossy" strip on an otherwise perfectly conducting plane surface is treated by an exact method employing elliptic wave functions. The calculations of the scattered fields of the strip by the two methods indicate the extent of the validity of the initial assumption in the approximate procedure.

INTRODUCTION

In most boundary value problems that arise in nature it is often very difficult to obtain an exact solution in usable form. One method often used for boundaries at imperfectly conducting media is to assume that the surface currents are the same as if the media were perfectly conducting. This approximation enables rather simple solutions to be obtained for a large class of problems. A particular example of some practical importance is the problem of a vertical antenna over a radial-wire mat lying on an imperfectly conducting ground. In the calculation of the power absorbed in the ground it is usually assumed that the total surface currents within a few wavelengths of the base of the antenna are the same as if the ground were perfectly conducting (6). This is equivalent to stating that the tangential magnetic field is independent of the ground conductivity if the latter is sufficiently high. This perturbation type of approximation has also been employed to calculate the attenuation in a wave guide (2) due to the imperfect conductivity of the walls. The same technique has been formulated recently, in a very general way, by Monteath (4) who pointed out a number of interesting applications.

One possible way to estimate the accuracy of this procedure is to compare the results for a particular problem solved both by the above-mentioned approximate method and by a more exact method. The problem chosen for this illustration is a two-dimensional one. The source is a line element of harmonically varying current situated above and parallel to a plane surface which has a one-dimensionally varying surface impedance.

APPROXIMATE METHOD OF SOLUTION

In this section the problem of a line source of current over a conducting half-plane with a lossy strip is formulated. The solution employing a perturbation type of approximation is then carried out.

The surface of the half-space is defined by $y = 0$ with reference to cartesian

[1]*Manuscript received April 1, 1955.*
Contribution from Radio Physics Laboratory, Defence Research Board, Ottawa, Ontario.
[2]*Present address: Central Radio Propagation Laboratory, Boulder, Colorado.*

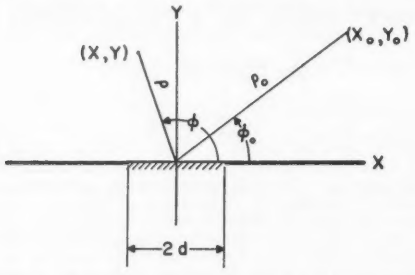

FIG. 1. "Lossy" strip on conducting plane and the coordinate system.

coordinates (x, y, z). The line source of current I is located at (x_0, y_0, z). The space $y > 0$ is homogeneous with electrical constants ϵ and μ whereas the surface of the lower medium is to have a specified inhomogeneous boundary condition such that

$$E_z = -\eta(x)H_x \quad \text{at } y = 0. \tag{1}$$

In other words the surface is assumed to exhibit the property of surface impedance (4). This type of boundary condition is quite useful in treating problems of absorption of radio waves in soils, at low frequencies. The factor of proportionality $\eta(x)$ has been termed the surface impedance and it is considered to be a function of x in this problem.

It is convenient to write the electric field as

$$E_z = E_z^{\infty} + E_z^s, \tag{2}$$

where E_z^{∞} is the field of the line source over a perfectly conducting half-space (i.e., $\eta(x) = 0$) and E_z^s is regarded as a correction term. Since E_z^s is a solution of Maxwell's equations, it can be written as a Fourier integral as follows:

$$E_z^s(x, y) = \int_{-\infty}^{+\infty} e^{-(\lambda^2-\beta^2)^{\frac{1}{2}}y} A(\lambda)\, e^{i\lambda x} d\lambda \quad \text{for } y \geqslant 0, \tag{3}$$

where $\beta = (\epsilon\mu)^{\frac{1}{2}}\omega$ and $A(\lambda)$ is a function to be determined from the conditions of the problem. Employing the inverse property of the Fourier transforms it follows that

$$A(\lambda) = \frac{1}{2\pi}\int_{-\infty}^{+\infty} E_z^s(\alpha, 0)\, e^{-i\lambda\alpha} d\alpha. \tag{4}$$

Invoking the boundary condition, equation [3] can now be rewritten

$$E_z^s(x, y) = -\frac{1}{2\pi}\int_{-\infty}^{+\infty}\int_{-\infty}^{+\infty} e^{-(\lambda^2-\beta^2)^{\frac{1}{2}}y} e^{i\lambda(x-\alpha)} \eta(\alpha)\, H_x(\alpha, 0)\, d\alpha d\lambda. \tag{5}$$

The integration with respect to λ can be carried out (1) to give

$$E_z^s(x, y) = \frac{-i\beta y}{\pi}\int_{-\infty}^{+\infty} \eta(\alpha)\, \frac{K_1[i\beta\sqrt{\{(x-\alpha)^2+y^2\}}]}{\sqrt{\{(x-\alpha)^2+y^2\}}} H_x(\alpha, 0)\, d\alpha, \tag{6}$$

where K_1 is the modified Bessel function of the second type. The approximation is now made that the tangential magnetic field $H_x(\alpha, 0)$ can be replaced by

the corresponding tangential magnetic field $H_x^{\infty}(\alpha, 0)$. In other words, it is assumed that surface currents are the same as if the plane were perfectly conducting.

When the fields are to be observed at a large distance from the plane $y = 0$, the Bessel function K_1 in equation [6] can be replaced by its asymptotic form, so that

$$[7] \qquad E_z^s \simeq -\left(\frac{\pi}{2i\beta\rho}\right)^{\frac{1}{2}} \frac{i\beta y}{\pi\rho} \int_{-\infty}^{+\infty} e^{i\beta\alpha\cos\phi}\eta(\alpha)\, e^{-i\beta\rho} H_x^{\infty}(\alpha, 0)\, d\alpha,$$

where it has been assumed that $x^2+y^2 \gg \alpha^2$ over the significant range of α, where $\rho = (x^2+y^2)^{\frac{1}{2}}$, and $\phi = \tan^{-1}(y/x)$. Now if the line source is also sufficiently far removed from $y = 0$, the incident wave is essentially plane and therefore

$$[8] \qquad H_x(\alpha, 0) \simeq H_x^{\infty}(\alpha, 0) = \frac{-2 \sin \phi_0\, E_0 e^{i\beta\alpha\cos\phi_0}}{\eta_0},$$

where $\phi_0 = \tan^{-1}(y_0/x_0)$, $\eta_0 = (\mu/\epsilon)^{\frac{1}{2}}$, and E_0 is the electric field of the incident wave at $x = 0$, $y = 0$. The secondary or scattered field E_z^s is then written conveniently as

$$[9] \qquad E_z^s = E_0 \frac{e^{-i\beta\rho}}{(\beta\rho)^{\frac{1}{2}}} T(\phi),$$

where

$$[10] \qquad T(\phi) = \beta(2i/\pi)^{\frac{1}{2}} \sin\phi \sin\phi_0 \int_{-\infty}^{+\infty} [\eta(\alpha)/\eta_0]\, e^{i\beta(\cos\phi+\cos\phi_0)\alpha} d\alpha.$$

If $y = 0$ is the boundary at a conducting medium, such as the earth's surface, the displacement currents are usually negligible at radio frequencies compared with the conduction currents and $\eta(\alpha)$ has a phase angle of 45°. As an example, the surface $y = 0$ is taken to be perfectly conducting everywhere except in a strip of width $2d$ where it has a high but finite conductivity such that

$$\eta(x)/\eta_0 = e^{i\pi/4} p_0 \text{ for } |x| < d,$$
$$= 0 \text{ for } |x| > d,$$

where p_0 is real when displacement currents are neglected. It then follows that

$$[11] \qquad T(\phi) = T_0(\phi) \simeq i2(2/\pi)^{\frac{1}{2}} \sin\phi \sin\phi_0\, p_0 \frac{\sin[\beta d(\cos\phi + \cos\phi_0)]}{(\cos\phi + \cos\phi_0)},$$

where the subscript zero on T is to indicate that the strip has a constant surface impedance.

Another case of interest is when the surface impedance varies across the strip. Although various forms could be chosen it is particularly worth while to select the functional form of $\eta(\alpha)$ as employed in the next section for a more exact analysis of the problem. The surface impedance function is taken as

$$\eta(\alpha)/\eta_0 = e^{i\pi/4}p[1-(x/d)^2]^{\frac{1}{2}} \text{ for } |x| < d,$$
$$= 0 \text{ for } |x| > d.$$

After a change of variable, equation [10] takes the form

$$[12] \quad T(\phi) = \sin\phi \sin\phi_0\, i\beta d(2/\pi)^{\frac{1}{2}}p \int_0^{\pi} e^{-i\beta d(\cos\phi+\cos\phi_0)\cos\theta}\sin^2\theta\, d\theta$$

which can be expressed in terms of the Bessel function of the first type of order unity (3). This leads to

$$[13] \quad T(\phi) = i(2\pi)^{\frac{1}{2}}p \sin\phi \sin\phi_0 \frac{J_1[\beta d(\cos\phi + \cos\phi_0)]}{(\cos\phi + \cos\phi_0)}.$$

It should be noted that the average value of $|\eta(\alpha)/\eta_0|$ across the varying strip is $p\pi/4$. The magnitude of the function $T(\phi)$ is plotted in Figs. 2 to 5 for $\beta d = 3$, for both the constant strip and the varying strip. The values of p_0 selected are $\pi/400$ and $\pi/40$ and the values of p are 0.01 and 0.10. It can

FIG. 2

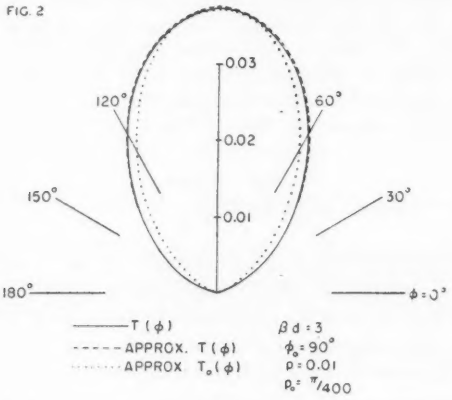

FIG. 3

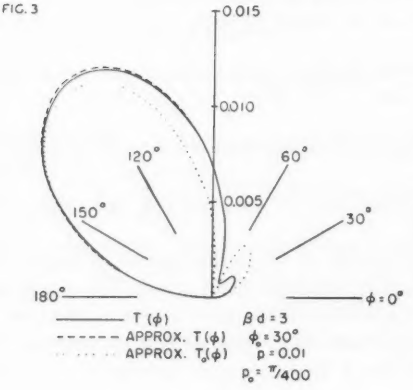

FIG. 4

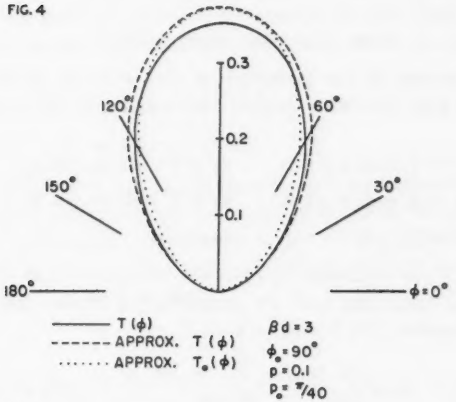

FIG. 5

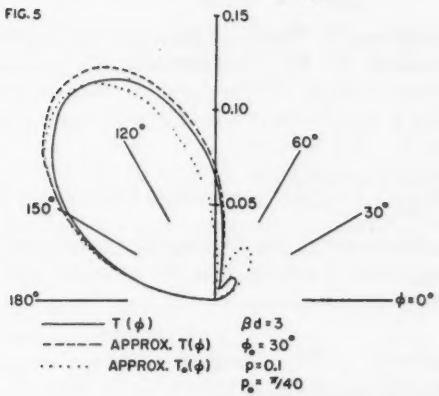

be seen that there is a close resemblance between the two cases of the constant and varying strips when p_0 is equal to the average value of p. It is also interesting to note that the energy scattered by the lossy strip is quite diffuse but has a general maximum in the forward and upward direction. For low angles of incidence the scattered field is greatly reduced in magnitude.

WAVE SOLUTION

A more exact method is now employed for calculating the scattered field from the strip. The line source is again taken to be at (x_0, y_0). The field E_z^{∞}, which has the proper singularity at x_0, y_0, and is a solution of the wave equation, is seen to be

$$E_z^{\infty} = \tfrac{1}{4}\mu\omega I[H_0^{(2)}(\beta\rho_1) - H_0^{(2)}(\beta\rho_1')], \tag{14}$$

where $H_0^{(2)}$ is the Hankel function of the second kind, of order zero,

$$\rho_1 = [(x-x_0)^2+(y-y_0)^2]^{\frac{1}{2}},$$

and

$$\rho_1' = [(x-x_0)^2+(y+y_0)^2]^{\frac{1}{2}}.$$

Considering the nature of the geometry of the problem, elliptic coordinates (u, v) are chosen with foci at $x = \pm d$. The equations of transformation are then

$$\begin{aligned} x &= d \cosh u \cos v, & x_0 &= d \cosh u_0 \cos v_0, \\ y &= d \sinh u \sin v, & y_0 &= d \sinh u_0 \sin v_0, \\ z &= z, & z_0 &= z_0. \end{aligned} \tag{15}$$

Solutions of the wave equation in elliptic coordinates can be expressed in terms of Mathieu functions and, by employing a known addition theorem for the Hankel function (5), it can be seen that

$$E_z^{\infty} = 2\mu\omega I \sum_{m=1}^{\infty} \frac{So_m(\beta d, v_0)\ So_m(\beta d, v)}{N_m^0(\beta d)} Jo_m(\beta d, u)\, Ho_m^{(2)}(\beta d, u_0), \tag{16}$$

where So_m are the odd angular Mathieu functions, Jo_m and $Ho_m^{(2)}$ are the odd radial Mathieu functions, and N_m^0 is the normalization parameter. The notation is essentially that of Morse and Feshbach (5). Remembering that $E_z^s = 0$ for $v = 0$ and π when $u > 0$ and that it is to be an outgoing wave at infinity, it can be expressed as

$$E_z^s = 2\mu\omega I \sum_{m=1}^{\infty} \frac{A_m So_m(\beta d, v_0)}{N_m^0(\beta d)} So_m(\beta d, v)\, Ho_m^{(2)}(\beta d, u_0)\, Ho_m^{(2)}(\beta d, u), \tag{17}$$

where A_m is to be determined from the boundary condition at $u = 0$. Now, from Maxwell's equations, it follows that the magnetic field component in the direction of increasing v is

$$H_v = -\frac{i}{\mu\omega h} \frac{\partial E_z}{\partial u}, \tag{18}$$

where h is a metrical coefficient given by

$$h = (\cosh^2 u - \cos^2 v)^{\frac{1}{2}}.$$

The boundary condition is now taken to be

$$[E_z(u, v) = \eta(v) H_v(u, v)]_{u=0}, \tag{19}$$

which is equivalent to

$$E_z(0, v) = -\frac{i}{\mu\omega} \frac{\eta(v)}{\sin v} \left[\frac{\partial E_z(u, v)}{\partial u}\right]_{u=0}. \tag{20}$$

Remembering that A_m must be independent of v for E_z^s to be a solution of the wave equation, it is seen that $\eta(v)/\sin v$ must be a constant. Therefore, if $\eta(v) = \eta_1 \sin v$,

$$A_m = \frac{Jo_m'(\beta d, 0)\eta_1}{i\beta d\eta_0 H_m^{(2)}(\beta d, 0) - \eta_1 Ho_m^{(2)'}(\beta d, 0)}, \tag{21}$$

where the prime on the radial function indicates a derivative with respect to

u evaluated at $u = 0$. In writing equation [21] in this form, the identity $Jo_m(\beta d, 0) = 0$ has been employed. This constitutes the exact solution of the problem for this particular boundary condition, which in terms of the coordinate x is

$$\eta(x) = \eta_1(1-x^2/d^2)^{\frac{1}{2}} \text{ for } |x| < d,$$
$$= 0 \text{ for } |x| > d.$$

This, of course, is the same functional form for $\eta(x)$ as discussed in the previous section. The distant scattered field from the strip can be obtained easily from equation [17] if the leading asymptotic forms of the radial functions $Ho_m^{(2)}$ are employed. Therefore, under the assumption that $\beta\rho$ and $\beta\rho_0$ are large compared with unity, it follows that

$$E_z^s = E_0 \frac{e^{-i\beta\rho}}{(\beta\rho)^{\frac{1}{2}}} T(\phi), \tag{22}$$

where

$$T(\phi) = 2(8\pi i)^{\frac{1}{2}} \sum_{m=1}^{\infty} \frac{(-1)^m p e^{-i\pi/4} Jo_m'(\beta d, 0) So_m(\beta d, \phi_0) So_m(\beta d, \phi)}{N_m^0(\beta d)[\beta d Ho_m^{(2)}(\beta d, 0) - p e^{-i\pi/4} Ho_m^{(2)'}(\beta d, 0)]} \tag{23}$$

and

$$\eta_1/\eta_0 = p e^{i\pi/4}.$$

The magnitude of the function $T(\phi)$ computed from equation [23] is shown plotted in Figs. 2 to 5 for the same range of p, βd, and ϕ_0 employed in the previous section. It is noticed that for the smaller value of p there is a close correspondence between the approximate curves and the more exact curves. When p is equal to 0.1 there is some difference, which however is not very appreciable. Calculations for larger values of p corresponding to a more poorly conducting strip indicate a considerable divergence between the approximate and exact formulae.

It is interesting to note that if equation [23] is developed into a power series in p, the first term can be readily shown to be identical to the approximate result for $T(\phi)$ given by equation [13].

CONCLUDING REMARKS

To facilitate the analysis in this paper, the source has been considered to be an infinite line of electric current. The radiation patterns calculated on the basis of this model are identical in form to the far field pattern in the equatorial plane of an antenna of finite length. The effect of the finite length of the strip is not expected to impair the patterns to any appreciable extent as long as the strip is at least twice as long as it is wide. This viewpoint has been substantiated experimentally in the study of slot radiators cut in rectangular metal plates (7), which in the sense of "Babinet's principle" is equivalent to the finite wire antenna parallel to the rectangular lossy strip.

The particular type of surface impedance variation discussed in the previous section could be considered a model to investigate the effect of horizontally polarized radio waves propagating over an inhomogeneous earth. In this case

the soil would be changing from a condition of very high conductivity at $|x| \geqslant d$ to a condition of somewhat poorer conductivity as $|x|$ approaches zero.

Finally, it can be concluded that the perturbation method of solution for scattering from a lossy strip on a conducting plane is justified if the strip is sufficiently well conducting. A criterion of its validity for this situation is that the magnitude of the surface impedance of the lossy regions of the plane should never exceed 0.1 times the intrinsic impedance of free space. It would therefore be expected that this perturbation technique is also a reasonable approximation for other problems which involve highly conducting surfaces having more complex distributions of surface impedance.

ACKNOWLEDGMENT

I would like to thank Miss M. O'Grady who carefully carried out the calculations.

REFERENCES

1. CAMPBELL, G. A. and FOSTER, R. M. Fourier integrals for practical applications. D. Van Nostrand Company Inc., New York. 1950. Pair No. 917.5.
2. LAMONT, R. L. Wave guides. Methuen and Co. Ltd., London. 1942. Chap. 3.
3. MCLACHLAN, N. W. Bessel functions for engineers. The Clarendon Press, Oxford. 1934. p. 158.
4. MONTEATH, G. D. Proc. Inst. Elect. Engrs. (London), Pt. IV, 98: 23. 1951.
5. MORSE, P. M. and FESHBACH, H. Methods of theoretical physics. McGraw-Hill Book Company, Inc., New York. 1953.
6. WAIT, J. R. and POPE, W. A. Appl. Sci. Research, B, 4: 177. 1954.
7. WAIT, J. R. and FROOD, D. G. Radio Physics Lab. Proj. Rept. 19-011. March 22, 1955.

A NOTE ON NUCLEAR TEMPERATURES AT LOW EXCITATION ENERGIES

By D. L. Livesey

Many nuclear reactions in which a compound nucleus is supposed to be formed are treated theoretically by statistical methods involving formulae for the average density of nuclear levels in a given region of excitation. In a simplified thermodynamic scheme the level density ω at excitation E is related to the density at zero excitation, ω_0, by the equation

$$\log_e(\omega/\omega_0) = S(E)/k$$

where the "nuclear entropy"

$$S(E)/k = \int dE/kT$$

and the "nuclear temperature" (kT) is determined by the nuclear equation of state. The model of a degenerate Fermi–Dirac gas yields the equation

$$E = a(kT)^2$$

and the well-known level-density formula

$$\log_e(\omega/\omega_0) = 2(aE)^{1/2}$$

where a is a constant of the order of $A/10$ Mev.$^{-1}$ if the nuclear radius is equal to $A^{1/3}.\ r_0$, with $r_0 = 1.4 \times 10^{-13}$ cm. Lang and Le Couteur (10) have pointed out that a formula of this type, with suitable refinements, is capable of explaining many experimental results in the region of nuclear excitation above 10 Mev. On the other hand, Cohen (3) has adduced evidence to indicate that, at low excitation energies, the effective nuclear temperature may actually decrease with increasing energy, an idea which runs counter to all thermodynamic principles. It is also known that the Fermi-gas formula with $a = A/10$ Mev.$^{-1}$ gives much too high values for level densities at moderate excitation in heavy nuclei if the observed values of ω_0 are employed.

It is the purpose of this note to point out that a number of experimental data relating to level densities can be brought together with the aid of a working hypothesis that the nuclear temperature is effectively constant for excitations below about 10 Mev., at a value given by the Fermi-gas equation of state close to 10 Mev. This temperature is of the order of $(100/A)^{1/2}$ Mev. for $r_0 = 1.4 \times 10^{-13}$ cm., but the value is not sensitive to the detailed assumptions made. The hypothesis is strongly suggested by the experiments of Gugelot (7) on the energy distributions of neutrons emitted in (p, n) reactions at high energies; and it may also explain certain features of the same author's results on protons inelastically scattered by various elements (8).

If the constant-temperature hypothesis is adopted, observed level densities in medium and heavy nuclei should obey the rule

$$\log_e(\omega/\omega_0) = E/kT$$

and this relation does, in fact, reproduce the behavior of heavy nuclei like W^{182} very well, when we consider the data of Fowler, Kruse, Keshishian, Klotz, and Mellor (6) and the spacing of slow-neutron resonances in such nuclei. Moreover, if the extensive data of Endt and Kluyver (5) on levels in fairly light nuclei are analyzed, it is found that, on the average, the level density increases according to a simple exponential law; the derived temperatures are rather higher than those expected, but this may be due to the existence of high-energy levels not yet detected.

If one applies the constant-temperature hypothesis to the problem of nucleons "evaporated" from highly-excited nuclei, e.g. in Gugelot's experiments or in photodisintegration processes, one expects the nucleon energy distribution $f(\eta)$ to be basically of the form

$$f(\eta) \cdot d\eta = \text{const.}\ \eta\, e^{-\eta/kT} \cdot d\eta$$

with suitable Coulomb-barrier corrections in the case of emitted protons. For example, the energy distribution of photoneutrons emitted by copper exposed to bremsstrahlung of maximum energy 70 Mev. has been determined by W. R. Dixon and the author, and the results are shown in the figure. The

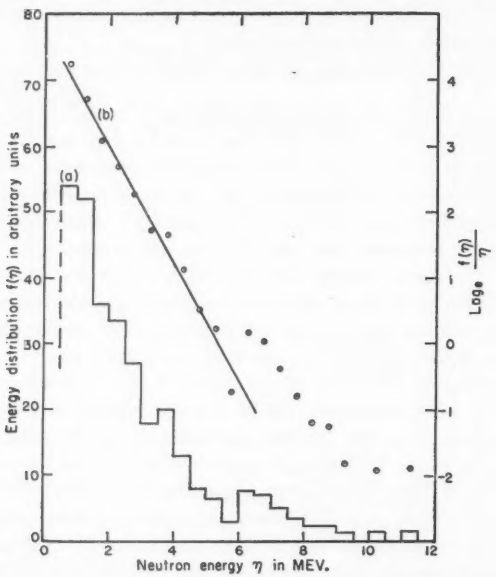

FIG. 1. Energy distribution of photoneutrons emitted from copper exposed to 70 Mev. bremsstrahlung. (*a*) Histogram based on 1000 tracks in nuclear emulsions. (*b*) Plot of $\log_e[f(\eta)/\eta]$ against neutron energy η.

shape of the distribution is very similar to that published by Byerly and Stephens (2) and the low-energy part obeys the above relation closely, as may be shown by plotting $\log_e[f(\eta)/\eta]$ against the neutron energy η. The straight line obtained indicates a nuclear temperature of 1.2 Mev., in agreement with the

$(100/A)^{1/2}$ formula. The data require correction for the effects of $(\gamma, 2n)$ reactions and for the shape of the (γ, n) excitation function, but these do not affect the results materially. A high-energy neutron component above 5 Mev. in the spectrum is probably due to direct-emission effects.

The same hypothesis used in the photoneutron work, with no further assumptions, is capable of explaining the main features of photoproton energy distributions obtained for aluminum by W. K. Dawson in this laboratory and for copper by Byerly and Stephens (2). It fails to account for the high-energy components of the photoprotons emitted by heavier elements, owing, no doubt, to the importance of direct-emission processes in these cases.

Although it is not easy to understand why an assembly of A nucleons should have an effectively constant temperature at low excitation energies, we might attempt to interpret the hypothesis in terms of Beard's suggestion (1) that the number of nucleons effective in excitation is less than the full value A below a certain degree of excitation. If this is so, the effective value of A must increase almost linearly from zero to its maximum value over the region 0 to 10 Mev. This may be an empirical method for taking into account the effects of shell-structure in the nucleus; these have been considered specifically by Margenau (11), who, however, dealt only with fluctuations on either side of the level densities predicted by the Fermi-gas formula. In this connection it may be significant that the calculations of Critchfield and Oleksa (4) on the level structure of Ne^{20}, based on the more recent shell theory, yield results which are at least consistent with a simple exponential increase of level density with excitation at low energies. Hurwitz and Bethe (9) have pointed out that the different types of nuclei require different treatment at low energies, and the whole concept of nuclear temperature is obviously of limited validity in this region. Nevertheless, it is clear from the experimental results that the simple hypothesis of a constant temperature is more satisfactory than any treatment based strictly on the Fermi–Dirac gas formula.

I must thank Dr. B. W. Sargent for extending to me the hospitality of this Department, and Dr. L. E. H. Trainor, Mr. W. R. Dixon, and Mr. W. K. Dawson for valuable discussions. The award of a Postdoctorate Fellowship by the National Research Council of Canada is gratefully acknowledged.

1. Beard, D. B. Phys. Rev. 94: 738. 1954.
2. Byerly, P. R. and Stephens, W. E. Phys. Rev. 83: 54. 1951.
3. Cohen, B. L. Phys. Rev. 92: 1245. 1953.
4. Critchfield, C. L. and Oleksa, S. Phys. Rev. 82: 243. 1951.
5. Endt, P. M. and Kluyver, J. C. Revs. Mod. Phys. 26: 95. 1954.
6. Fowler, C. M., Kruse, H. W., Keshishian, V., Klotz, R. J., and Mellor, G. P. Phys. Rev. 94: 1082. 1954.
7. Gugelot, P. C. Phys. Rev. 81: 51. 1951.
8. Gugelot, P. C. Phys. Rev. 93: 425. 1954.
9. Hurwitz, H. and Bethe, H. A. Phys. Rev. 81: 898. 1951.
10. Lang, J. M. B. and Le Couteur, K. J. Proc. Phys. Soc. (London), A, 67: 586. 1954.
11. Margenau, H. Phys. Rev. 59: 627. 1941.

Received March 7, 1955.
Physics Department,
Queen's University,
Kingston, Ontario.

THE EMISSION OF THE 'λ4050 Å' BANDS AND AN ASSOCIATED VIOLET CONTINUUM IN OXYACETYLENE FLAMES

By G. V. Marr and R. W. Nicholls

INTRODUCTION

Bands in the region of 4050 Å have been observed in emission in the spectra of comets (7) and in absorption in the spectra of N-Type stars (9). These bands have now been produced in the laboratory in emission in electrical discharges (6, 1, 4), hydrocarbon flames (2, 8, 3), carbon tube furnaces (12), and in absorption by flash photolysis (11). Attention has largely been confined to the identification of the molecule responsible for these bands and recently Clusius and Douglas (1) have definitely shown that this is the triatomic molecule C_3.

Swings, McKellar, and Rao (13) have pointed out that in stellar spectra these C_3 bands are accompanied by a strong continuous absorption extending into the ultraviolet. Herman and Herman (5) have reported a continuum found in the radiation from a discharge tube which produced the C_3 bands. This continuum has a maximum at about 4300 Å and was tentatively ascribed to the molecule CH. Phillips and Brewer (12) however describe a continuum with intensity maxima at 4000 Å and at 4300 Å associated with the production of the C_3 bands in a carbon tube furnace. The former maximum was shown by them to be emitted by C_3. McKellar and Richardson (10) have discussed the implications of these continua to stellar spectra.

As part of a program of intensity measurements on spectra of astrophysical interest, oxyhydrocarbon flames are being employed in this laboratory as low excitation energy sources. Following Kiess and Bass (8), the C_3 bands were readily excited in the luminous region of a fuel rich oxyacetylene flame. It is the purpose of this note to report the observation of a strong violet continuum associated with these bands, which appears similar to that reported by Phillips and Brewer. Preliminary photographic intensity measurements on spectra from different regions of the flame show strong correlations between the C_3 bands and the continuum.

EXPERIMENTAL

The oxyacetylene flame was burned on a commercial welding torch supplied through flowmeters with commercial oxygen and acetylene. A metal diaphragm with a horizontal aperture served to limit the region of the flame to be observed. Spectra were photographed on Kodak I-N plates using a Bausch and Lomb Littrow Spectrograph with a reciprocal dispersion of 4 Å/mm. at 4000 Å. Plate sensitivity calibrations were carried out with the aid of a Phillips Tungsten Filament Lamp and a rotating step sector. Relative intensity measurements were obtained by constant density photometry (14) of which more details will be published shortly.

RESULTS

In agreement with Kiess and Bass the C_3 bands were observed in the luminous region of the flame with fuel–oxygen ratios 2.5 to 4 times stoichiometric.

Fig. 1 shows a plot of relative intensity versus wavelength over the wavelength range of 3800 Å to 4500 Å for a flame whose fuel–oxygen ratio was 2.8 times stoichiometric and applies to the region about 3 mm. above the reaction zone. It will be observed that bands of CH, CN, C_2, and C_3 are

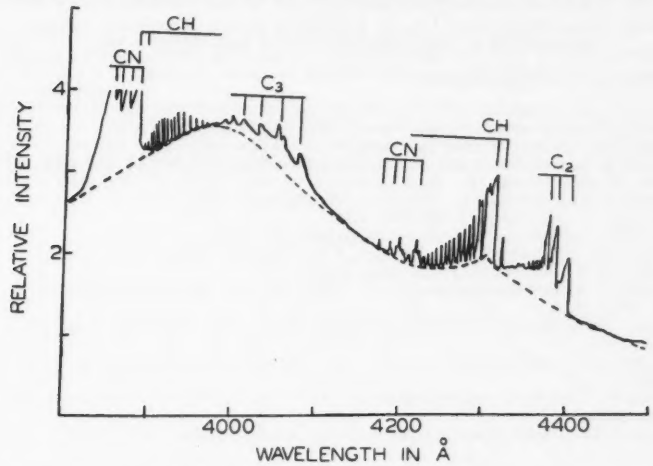

FIG. 1. The emission of the 'λ4050 Å' bands and an associated violet continuum in oxy-acetylene flames.

superimposed on a continuous background, the profile of which is indicated by the dotted curve. Intensity measurements made between the open rotational structure of CH bands enable a reasonably reliable profile to be determined except in the immediate vicinity of the C_3 bands.

In common with Phillips' and Brewer's observations maxima were observed at 4000 Å and 4300 Å though the CH band at 4313 Å makes the presence of the second maximum less certain.

DISCUSSION

The general features of Fig. 1 are very similar to the features reported by Phillips and Brewer for the emission spectrum from a carbon furnace at 2700°C. They investigated the variation of intensity with the concentration of molecules present and concluded that the broad maximum and continuous emission to the short wavelength side of 4000 Å was due to C_3.

The variation of relative intensities of the features of Fig. 1 with flame conditions is being studied. From the results so far obtained it appears that the C_3 bands are strongly associated with the continuum, and it has not been found possible to observe one without the other. Correlation between the intensity variations of the C_3 bands and bands of other emitters appears small. These observations favor the view held by Phillips and Brewer that C_3 is the emitter of at least a major portion of the continuum. More precise investigations are being made and will be reported later.

ACKNOWLEDGMENT

This work was partly supported by Contract AF 19(122)–470 with the U.S. Air Force Cambridge Research Centre and partly by a Research Grant from Imperial Oil Limited, both of which are gratefully acknowledged. The authors would also like to express their thanks to Dr. J. G. Phillips of the Berkeley Astronomy Department and Dr. A. McKellar of the Dominion Astrophysical Observatory, Royal Oak for discussions and making their results available to the authors prior to publication.

1. Clusius, K. and Douglas, A. E. Can. J. Phys. 32: 319. 1954.
2. Durie, R. A. Proc. Roy. Soc. (London), A, 211: 110. 1952.
3. Gaydon, A. G. and Wolfhard, H. G. Proc. Roy. Soc. (London), A, 213: 366. 1952.
4. Goupil, R. and Herman, R. Ann. astrophys. 16: 444. 1953.
5. Herman, R. and Herman, L. Compt. rend. 238: 664. 1954.
6. Herzberg, G. Astrophys. J. 96: 314. 1942.
7. Jose, P. D. and Swings, P. Astrophys. J. 111: 41. 1950.
8. Kiess, N. H. and Bass, A. M. J. Chem. Phys. 22: 569. 1954.
9. McKellar, A. Astrophys. J. 108: 453. 1948.
10. McKellar, A. and Richardson, E. H. Mém. soc. roy. sci. Liège, Collection in −8°, 15: 256. 1955.
11. Norrish, R. G. W., Porter, G., and Thrush, B. A. Proc. Roy. Soc. (London), A, 216: 165. 1953.
12. Phillips, J. G. and Brewer, L. Mém. soc. roy. sci. Liège, Collection in −8°, 15: 341. 1955.
13. Swings, P., McKellar, A., and Rao, K. N. Monthly Notices Roy. Astron. Soc. 113: 427. 1953.
14. Young, B. G. Thesis, University of Western Ontario, London, Ont. 1954.

Received March 21, 1955.
Department of Physics,
University of Western Ontario,
London, Canada.

LETTERS TO THE EDITOR

Under this heading brief reports of important discoveries in physics may be published. These reports should not exceed 600 words and, for any issue, should be submitted not later than six weeks previous to the first day of the month of issue. No proof will be sent to the authors.

The Velocity and Attenuation of Sound in Solid Argon

This letter is a preliminary report of measurements on the velocity and attenuation of sound in solid argon.

Solid argon is readily obtained by condensing the gas into a container which is maintained at the temperature of liquid nitrogen, 62°K.–78°K. In our measurements, a tube of barium titanate ceramic is filled with solid argon and the resonance frequencies of the enclosed plug of argon found by using one half of the ceramic as a transmitter and the other half as a receiver of acoustical energy (see Fig. 1).

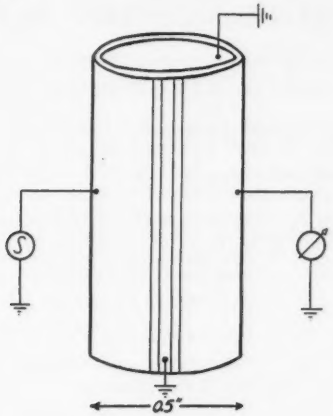

FIG. 1. The figure shows the electrical connections made on the ceramic. Only one of the two grounding strips is shown in the drawing.

The duality of the transducer is achieved by using the inner conducting surface as a common ground and dividing the outer conducting surface into two electrodes by vertical insulating strips which run the length of the ceramic. For electrical shielding, it is necessary and quite convenient to separate the two outer electrodes by grounding strips.

Such a transducer works well for liquids. The resonance frequencies of the system are found by noting the frequencies at which maximum response occurs. The sound velocities may then be calculated from the absolute frequencies or from the frequency differences. Successive frequencies give velocities readily consistent to within one part in 2000. This technique is less satisfactory when the cylinder is filled with solid argon. Difficulties arise from an apparently high attenuation, which we estimate to be 0.6 per cm. at 1.5 Mc. per sec. We find the velocity to be 1255±15 meters per sec. at 78°K. and 1322±15 meters per sec. at 64°K. These figures may be compared with 1300 and 1600 at 78°K. and 60°K. of Barker, Dobbs, and Jones (1).

The authors acknowledge the assistance of the National Research Council which is supporting this work with a grant in aid of research and with a postdoctorate fellowship held by C.K.H.

1. BARKER, J. R., DOBBS, E. R., and JONES, G. O. Phil. Mag. 44: 1182. 1953.

RECEIVED MAY 16, 1955.
DEPARTMENT OF PHYSICS,
DALHOUSIE UNIVERSITY,
HALIFAX, NOVA SCOTIA.

E. W. GUPTILL
C. K. HOYT
D. K. ROBINSON

CANADIAN JOURNAL OF PHYSICS

Notes to Contributors

Manuscripts

(i) ***General.*** Manuscripts, in English or French, should be typewritten, double spaced, on paper 8½×11 in. **The original and one copy are to be submitted.** Tables and captions for the figures should be placed at the end of the manuscript. Every sheet of the manuscript should be numbered.

Style, arrangement, spelling, and abbreviations should conform to the usage of this journal. Names of all simple compounds, rather than their formulas, should be used in the text. Greek letters or unusual signs should be written plainly or explained by marginal notes. Superscripts and subscripts must be legible and carefully placed.

Manuscripts should be carefully checked before they are submitted; authors will be charged for changes made in the proof that are considered excessive.

(ii) ***Abstract.*** An abstract of not more than about 200 words, indicating the scope of the work and the principal findings, is required, except in Notes.

(iii) ***References.*** References should be listed **alphabetically by authors' names,** numbered, and typed after the text. The form of the citations should be that used in this journal; in references to papers in periodicals, titles should not be given and only initial page numbers are required. All citations should be checked with the original articles and each one referred to in the text by the key number.

(iv) ***Tables.*** Tables should be numbered in roman numerals and each table referred to in the text. Titles should always be given but should be brief; column headings should be brief and descriptive matter in the tables confined to a minimum. Vertical rules should be used only when they are essential. Numerous small tables should be avoided.

Illustrations

(i) ***General.*** All figures (including each figure of the plates) should be numbered consecutively from 1 up, in arabic numerals, and each figure referred to in the text. The author's name, title of the paper, and figure number should be written in the lower left corner of the sheets on which the illustrations appear. Captions should not be written on the illustrations (see Manuscripts (i)).

(ii) ***Line Drawings.*** Drawings should be carefully made with India ink on white drawing paper, blue tracing linen, or co-ordinate paper ruled in blue only; any co-ordinate lines that are to appear in the reproduction should be ruled in black ink. Paper ruled in green, yellow, or red should not be used unless it is desired to have all the co-ordinate lines show. All lines should be of sufficient thickness to reproduce well. Decimal points, periods, and stippled dots should be solid black circles large enough to be reduced if necessary. Letters and numerals should be neatly made, preferably with a stencil (**do NOT use typewriting**) and be of such size that the smallest lettering will be not less than 1 mm. high when reproduced in a cut 3 in. wide.

Many drawings are made too large; originals should not be more than 2 or 3 times the size of the desired reproduction. In large drawings or groups of drawings the ratio of height to width should conform to that of a journal page but the height should be adjusted to make allowance for the caption.

The original drawings and one set of clear copies (e.g. small photographs) are to be submitted.

(iii) ***Photographs.*** Prints should be made on glossy paper, with strong contrasts. They should be trimmed so that essential features only are shown and mounted carefully, with rubber cement, on white cardboard with no space or only a **very** small space (less than 1 mm.) between them. In mounting, full use of the space available should be made (to reduce the number of cuts required) and the ratio of height to width should correspond to that of a journal page (4¼×7½ in.); however, allowance must be made for the captions. Photographs or groups of photographs should not be more than 2 or 3 times the size of the desired reproduction.

Photographs are to be submitted in duplicate; if they are to be reproduced in groups one set should be mounted, the duplicate set unmounted.

Reprints

A total of 50 reprints of each paper, without covers, are supplied free. Additional reprints, with or without covers, may be purchased.

Charges for reprints are based on the number of printed pages, which may be calculated approximately by multiplying by 0.6 the number of manuscript pages (double-spaced typewritten sheets, 8½×11 in.) and including the space occupied by illustrations. An additional charge is made for illustrations that appear as coated inserts. The cost per page is given on the reprint requisition which accompanies the galley.

Any reprints required in addition to those requested on the author's reprint requisition form must be ordered officially as soon as the paper has been accepted for publication.

Contents

Printed in Canada *by* University of Toronto Press